Verification of radome problems - Part I

Kristensson, Gerhard

2018

Document Version:
Publisher's PDF, also known as Version of record

CODEN:LUTEDX/(TEAT-7262)/1-30/(2018)

Verification of radome problems — Part I

Gerhard Kristensson

Electromagnetic Theory
Department of Electrical and Information Technology
Lund University
Sweden

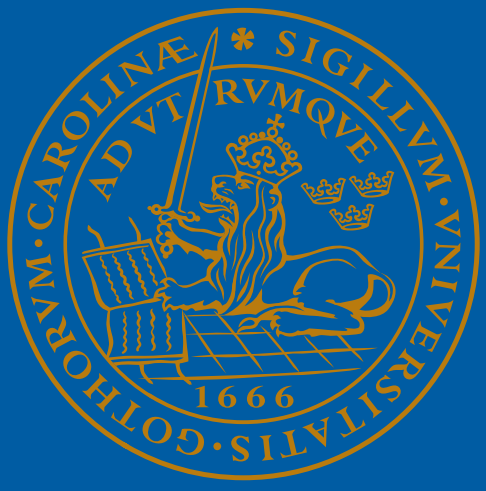

(TEAT-7262)/1-30/(2018): G. Kristensson, Verification of radome problems — Part I

Gerhard Kristensson
gerhard.kristensson@eit.lth.se

Department of Electrical and Information Technology
Electromagnetic Theory
Lund University
P.O. Box 118
SE-221 00 Lund
Sweden

Editor: Mats Gustafsson

Abstract

This paper contains the analysis of the transmission problem with a spherical, dielectric (possibly lossy) shell. The sources to the problem are located inside the spherical, dielectric shell. Two different source configurations are investigated — an off-center located electric dipole and a circular Huygens surface. An exact modal series solution of the transmission problem is found and the solution is numerically illustrated for a series of shell thicknesses. The accuracy of the solution is tested by a power balance computation, which typically gives at least 10 significant figures.

1 Introduction

The aim of this paper is to develop an exact modal series solution to the radiation problem of a given source configuration in the presence of a radome. The most simple geometry accessible for this purpose is that of a spherical geometry. The geometry might not be a candidate for a real radome construction, but it serves as an excellent verification case for various numerical implementations of electromagnetic problems that rely on approximations. This enables an accurate comparison of these approximations with the results of this spherical case, which is solved with high accuracy.

The solution to this problem of spherical geometry is found by separation of variables, and the solutions in the different regions are found in terms of spherical vector waves [3]. Two different sources are investigated — the simple off-centered electrical dipole and a disk with prescribed electric and magnetic surface fields. To avoid degradation in the accuracy of the solution, all involved integral must be solved with machine precision. To this end, no integrals that appear in this paper are solved by numerical integration, but as finite sums of special functions, which can be calculated with machine precision. An advantage with the analysis presented in this paper is that the accuracy of the method can be stated. In general, at least 11–13 significant digits are obtained.

The plan of the paper is as follows: In Section 2, we solve the transmission problem with a general source configuration. The solution is illustrated with a vertical electric elementary dipole and a circular disk with constant surface fields (Huygens surface) in Sections 3 and 4, respectively. Some conclusions of the paper are found in Section 5, and the paper ends with three appendices that contain definitions and exact evaluations of the pertinent integrals that appear in Sections 3 and 4.

2 Special radome problem — spherical shell

In this section, we adopt a simple canonical geometry, a spherical shell of inner radius a and outer radius b, see Figures 1 and 2, as a way to verify the errors made with geometrical optics and iterative physical optics codes. In general, all three

regions of the setup have different material parameters, but in most applications the material inside and outside the spherical shell are the same.

2.1 Expansions of the fields

We divide the geometry into four different regions, see Figures 1 and 2:

1. The region inside the spherical shell and inside the smallest circumscribed sphere (centered at the origin) of the sources (this region has material parameters ϵ_1 and μ_1 and wave number k_1)

2. The region inside the spherical shell and outside the smallest circumscribed sphere (centered at the origin) of the sources (this region has material parameters ϵ_1 and μ_1 and wave number k_1)

3. The region inside the spherical shell with material parameters ϵ_2 and μ_2 and wave number k_2

4. The region outside the spherical shell with real-valued material parameters ϵ and μ and wave number k

In each region, we expand the field in spherical vector waves, outgoing $\boldsymbol{u}_n(k\boldsymbol{r})$ and regular $\boldsymbol{v}_n(k\boldsymbol{r})$, respectively, see Appendix A and [3, Chap. 7] for their definitions.

The pertinent expansions of the electric fields in the four regions are (note the appropriate wave number in the various expansions)

$$\begin{cases} \boldsymbol{E}_{\rm exc}(\boldsymbol{r}) = \sum_n a_n \boldsymbol{u}_n(k_1\boldsymbol{r}), \quad d < r < a \\ \boldsymbol{E}_{\rm ref}(\boldsymbol{r}) = \sum_n r_n a_n \boldsymbol{v}_n(k_1\boldsymbol{r}), \quad 0 \le r < a \\ \boldsymbol{E}_1(\boldsymbol{r}) = \sum_n \alpha_n \boldsymbol{v}_n(k_2\boldsymbol{r}) + t_n \alpha_n \boldsymbol{u}_n(k_2\boldsymbol{r}), \quad a < r < b \\ \boldsymbol{E}_{\rm t}(\boldsymbol{r}) = \sum_n f_n \boldsymbol{u}_n(k\boldsymbol{r}), \quad r > b \end{cases}$$

Here, the index n denotes a four index set $n = \{\tau, \sigma, l, m\}$, $\tau = 1, 2$, $\sigma = \mathrm{e}, \mathrm{o}$, $m = 0, 1, \ldots, l$, and $l = 1, 2, \ldots$, see [3]. Below, we also adopt a three index set $n = \{\sigma, l, m\}$. The field $\boldsymbol{E}_{\rm exc}(\boldsymbol{r})$ is the excitation field without the spherical shell. This field is prescribed and fixed. The field $\boldsymbol{E}_{\rm ref}(\boldsymbol{r})$ is the field that is reflected by the spherical radome. The total field inside the spherical shell, $d < r < a$, is the sum of these two fields, *i.e.*, $\boldsymbol{E}_{\rm int}(\boldsymbol{r}) = \boldsymbol{E}_{\rm exc}(\boldsymbol{r}) + \boldsymbol{E}_{\rm ref}(\boldsymbol{r})$. The field $\boldsymbol{E}_1(\boldsymbol{r})$ is the total field inside the spherical shell, and $\boldsymbol{E}_{\rm t}(\boldsymbol{r})$ is the field that is transmitted to the exterior region. The difference between the fields $\boldsymbol{E}_{\rm exc}(\boldsymbol{r})$ and $\boldsymbol{E}_{\rm int}(\boldsymbol{r}) = \boldsymbol{E}_{\rm exc}(\boldsymbol{r}) + \boldsymbol{E}_{\rm ref}(\boldsymbol{r})$ demonstrates the effect of the radome.

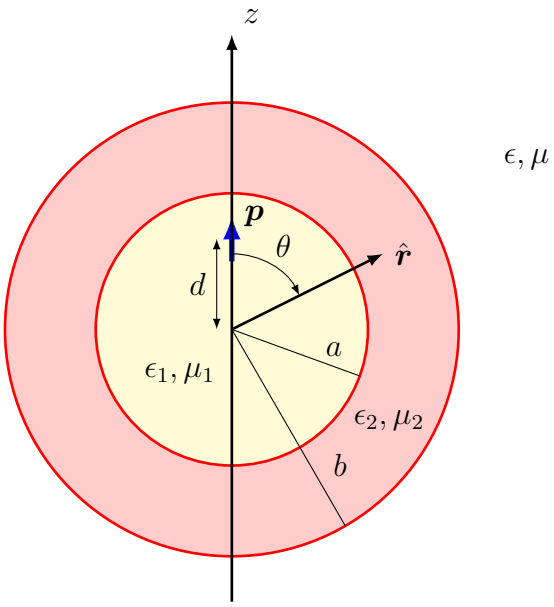

Figure 1: The geometry of the transmission problem of a vertical electric dipole $\boldsymbol{p}$ inside a spherical shell. The dipole is located at $d\hat{\boldsymbol{z}}$.

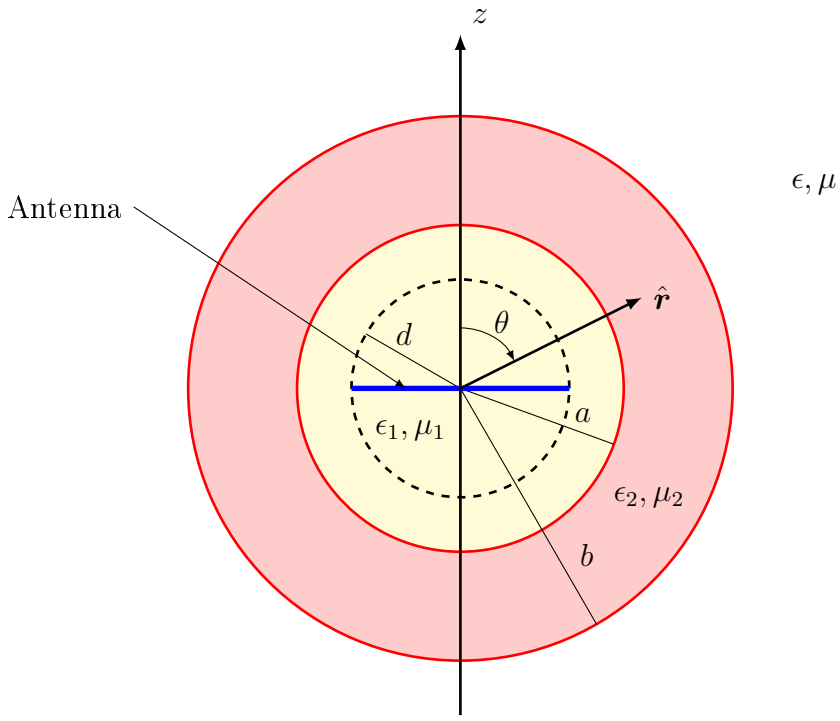

Figure 2: The geometry of the transmission problem of a circular disk of radius d inside a spherical shell of inner radius a and outer radius b. The the smallest circumscribed sphere of the disk has the radius $d < a$.

The corresponding magnetic fields are

$$\begin{cases} \mathrm{i}\eta_1\eta_0 \boldsymbol{H}_{\mathrm{exc}}(\boldsymbol{r}) = \sum_n a_n \boldsymbol{u}_{\overline{n}}(k_1\boldsymbol{r}), & d < r < a \\ \mathrm{i}\eta_1\eta_0 \boldsymbol{H}_{\mathrm{ref}}(\boldsymbol{r}) = \sum_n r_n a_n \boldsymbol{v}_{\overline{n}}(k_1\boldsymbol{r}), & 0 \leq r < a \\ \mathrm{i}\eta_2\eta_0 \boldsymbol{H}_1(\boldsymbol{r}) = \sum_n \alpha_n \boldsymbol{v}_{\overline{n}}(k_2\boldsymbol{r}) + t_n\alpha_n \boldsymbol{u}_{\overline{n}}(k_2\boldsymbol{r}), & a < r < b \\ \mathrm{i}\eta\eta_0 \boldsymbol{H}_{\mathrm{t}}(\boldsymbol{r}) = \sum_n f_n \boldsymbol{u}_{\overline{n}}(k\boldsymbol{r}), & r > b \end{cases}$$

where η_0 is the wave impedance of vacuum, and η_1, η_2, and η are the relative wave impedance for the corresponding material, and where we have introduced the dual index $\overline{n} = \{\overline{\tau}\sigma ml\}$, where the dual index to τ is defined by $\overline{1} = 2$ and $\overline{2} = 1$.

The electric and magnetic fields inside the spherical shell, but outside the inscribed sphere of the sources, are

$$\boldsymbol{E}_{\mathrm{int}}(\boldsymbol{r}) = \boldsymbol{E}_{\mathrm{exc}}(\boldsymbol{r}) + \boldsymbol{E}_{\mathrm{ref}}(\boldsymbol{r}), \quad \boldsymbol{H}_{\mathrm{int}}(\boldsymbol{r}) = \boldsymbol{H}_{\mathrm{exc}}(\boldsymbol{r}) + \boldsymbol{H}_{\mathrm{ref}}(\boldsymbol{r}), \quad d < r < a$$

Note that we assume that the generating sources are fixed, and not altered by the presence of the spherical shell. Consequently, we have simplified the problem, and we do not account for the effects made by the shell on the sources inside the spherical shell.

2.2 Solution of the radiation problem

The boundary conditions on $r = a$ and $r = b$, *i.e.*, $\hat{\boldsymbol{r}} \times \boldsymbol{E}$ and $\hat{\boldsymbol{r}} \times \boldsymbol{H}$ continuous on these surfaces, imply for $\tau = 1$

$$\begin{cases} a_{1l}\left(\xi_l(k_1a) + r_{1l}\psi_l(k_1a)\right) = \dfrac{k_1}{k_2}\alpha_{1l}\left(\psi_l(k_2a) + t_{1l}\xi_l(k_2a)\right) \\ a_{1l}\left(\xi_l'(k_1a) + r_{1l}\psi_l'(k_1a)\right) = \dfrac{k_1\eta_1}{k_2\eta_2}\alpha_{1l}\left(\psi_l'(k_2a) + t_{1l}\xi_l'(k_2a)\right) \\ \alpha_{1l}\left(\psi_l(k_2b) + t_{1l}\xi_l(k_2b)\right) = \dfrac{k_2}{k} f_{1l}\xi_l(kb) \\ \alpha_{1l}\left(\psi_l'(k_2b) + t_{1l}\xi_l'(k_2b)\right) = \dfrac{k_2\eta_2}{k\eta} f_{1l}\xi_l'(kb) \end{cases}$$

and for $\tau = 2$, the boundary conditions give

$$\begin{cases} a_{2l}\left(\xi_l'(k_1a) + r_{2l}\psi_l'(k_1a)\right) = \dfrac{k_1}{k_2}\alpha_{2l}\left(\psi_l'(k_2a) + t_{2l}\xi_l'(k_2a)\right) \\ a_{2l}\left(\xi_l(k_1a) + r_{2l}\psi_l(k_1a)\right) = \dfrac{k_1\eta_1}{k_2\eta_2}\alpha_{2l}\left(\psi_l(k_2a) + t_{2l}\xi_l(k_2a)\right) \\ \alpha_{2l}\left(\psi_l'(k_2b) + t_{2l}\xi_l'(k_2b)\right) = \dfrac{k_2}{k} f_{2l}\xi_l'(kb) \\ \alpha_{2l}\left(\psi_l(k_2b) + t_{2l}\xi_l(k_2b)\right) = \dfrac{k_2\eta_2}{k\eta} f_{2l}\xi_l(kb) \end{cases}$$

where $\xi_l(z)$ and $\psi_l(z)$ are the Riccati-Bessel functions (for their definitions, see Appendix A and [3, App. B.3.3]). Divide the equations with each other pairwise.

$$\begin{cases} \dfrac{\xi_l(k_1a) + r_{1l}\psi_l(k_1a)}{\xi_l'(k_1a) + r_{1l}\psi_l'(k_1a)} = \dfrac{\eta_2}{\eta_1}\dfrac{\psi_l(k_2a) + t_{1l}\xi_l(k_2a)}{\psi_l'(k_2a) + t_{1l}\xi_l'(k_2a)} = A_{1l} \\ \dfrac{\psi_l(k_2b) + t_{1l}\xi_l(k_2b)}{\psi_l'(k_2b) + t_{1l}\xi_l'(k_2b)} = \dfrac{\eta}{\eta_2}\dfrac{\xi_l(kb)}{\xi_l'(kb)} \end{cases}$$

and

$$\begin{cases} \dfrac{\xi_l'(k_1a) + r_{2l}\psi_l'(k_1a)}{\xi_l(k_1a) + r_{2l}\psi_l(k_1a)} = \dfrac{\eta_2}{\eta_1}\dfrac{\psi_l'(k_2a) + t_{2l}\xi_l'(k_2a)}{\psi_l(k_2a) + t_{2l}\xi_l(k_2a)} = A_{2l} \\ \dfrac{\psi_l'(k_2b) + t_{2l}\xi_l'(k_2b)}{\psi_l(k_2b) + t_{2l}\xi_l(k_2b)} = \dfrac{\eta}{\eta_2}\dfrac{\xi_l'(kb)}{\xi_l(kb)} \end{cases}$$

Solve for $r_{\tau l}$ and $t_{\tau l}$. The result is

$$\begin{cases} r_{1l} = -\dfrac{A_{1l}\xi_l'(k_1a) - \xi_l(k_1a)}{A_{1l}\psi_l'(k_1a) - \psi_l(k_1a)} \\ t_{1l} = -\dfrac{\xi_l(kb)\psi_l'(k_2b) - \frac{\eta_2}{\eta}\xi_l'(kb)\psi_l(k_2b)}{\xi_l(kb)\xi_l'(k_2b) - \frac{\eta_2}{\eta}\xi_l'(kb)\xi_l(k_2b)} \end{cases}$$

and

$$\begin{cases} r_{2l} = -\dfrac{A_{2l}\xi_l(k_1a) - \xi_l'(k_1a)}{A_{2l}\psi_l(k_1a) - \psi_l'(k_1a)} \\ t_{2l} = -\dfrac{\xi_l'(kb)\psi_l(k_2b) - \frac{\eta_2}{\eta}\xi_l(kb)\psi_l'(k_2b)}{\xi_l'(kb)\xi_l(k_2b) - \frac{\eta_2}{\eta}\xi_l(kb)\xi_l'(k_2b)} \end{cases}$$

There is some resemblance between the transition matrix elements of a dielectric sphere, see (8.7) on page 420 in [3], and the coefficients $t_{\tau l}$ above. Note that the factors $A_{\tau l}$ contain the factors $t_{\tau l}$, which are explicitly given by the second expression. Finally, the unknowns $f_{\tau l}$ and $\alpha_{\tau l}$ are solved in the known $r_{\tau l}$ and $t_{\tau l}$. We get

$$\begin{cases} \alpha_{1l} = \dfrac{k_2}{k_1}\dfrac{\xi_l(k_1a) + r_{1l}\psi_l(k_1a)}{\psi_l(k_2a) + t_{1l}\xi_l(k_2a)}a_{1l} \\ f_{1l} = \dfrac{k}{k_2}\dfrac{\psi_l(k_2b) + t_{1l}\xi_l(k_2b)}{\xi_l(kb)}\alpha_{1l} \end{cases}$$

and

$$\begin{cases} \alpha_{2l} = \dfrac{k_2}{k_1}\dfrac{\xi_l'(k_1a) + r_{2l}\psi_l'(k_1a)}{\psi_l'(k_2a) + t_{2l}\xi_l'(k_2a)}a_{2l} \\ f_{2l} = \dfrac{k}{k_2}\dfrac{\psi_l'(k_2b) + t_{2l}\xi_l'(k_2b)}{\xi_l'(kb)}\alpha_{2l} \end{cases}$$

The transmission problem is now formally solved, but some simplifications can be made with the use of the Wronskian for the Riccati-Bessel functions, $\psi_l(z)\xi_l'(z) - \psi_l'(z)\xi_l(z) = \mathrm{i}$ [3, App. B.3.3]. In fact, the numerators in the expression of $\alpha_{\tau l}$ and

$f_{\tau l}$ contain the expressions

$$\begin{cases} \xi_l(k_1 a) + r_{1l}\psi_l(k_1 a) = -\dfrac{\mathrm{i}A_{1l}}{A_{1l}\psi_l'(k_1 a) - \psi_l(k_1 a)} \\ \psi_l(k_2 b) + t_{1l}\xi_l(k_2 b) = \dfrac{\mathrm{i}\xi_l(kb)}{\xi_l(kb)\xi_l'(k_2 b) - \frac{\eta_2}{\eta}\xi_l'(kb)\xi_l(k_2 b)} \end{cases}$$

and

$$\begin{cases} \xi_l'(k_1 a) + r_{2l}\psi_l'(k_1 a) = \dfrac{\mathrm{i}A_{2l}}{A_{2l}\psi_l(k_1 a) - \psi_l'(k_1 a)} \\ \psi_l'(k_2 b) + t_{2l}\xi_l'(k_2 b) = -\dfrac{\mathrm{i}\xi_l'(kb)}{\xi_l'(kb)\xi_l(k_2 b) - \frac{\eta_2}{\eta}\xi_l(kb)\xi_l'(k_2 b)} \end{cases}$$

These expressions simplify the values of $\alpha_{\tau l}$ and $f_{\tau l}$.

$$\begin{cases} \alpha_{1l} = -\dfrac{k_2}{k_1}\dfrac{\mathrm{i}A_{1l}a_{1l}}{\left(A_{1l}\psi_l'(k_1 a) - \psi_l(k_1 a)\right)\left(\psi_l(k_2 a) + t_{1l}\xi_l(k_2 a)\right)} \\ f_{1l} = \dfrac{\mu}{\mu_1}\dfrac{1}{\frac{\eta}{\eta_2}\xi_l(kb)\xi_l'(k_2 b) - \xi_l'(kb)\xi_l(k_2 b)} \\ \qquad \cdot \dfrac{a_{1l}}{\left(A_{1l}\psi_l'(k_1 a) - \psi_l(k_1 a)\right)\left(\psi_l'(k_2 a) + t_{1l}\xi_l'(k_2 a)\right)} \end{cases}$$

and

$$\begin{cases} \alpha_{2l} = \dfrac{k_2}{k_1}\dfrac{\mathrm{i}A_{2l}a_{2l}}{\left(A_{2l}\psi_l(k_1 a) - \psi_l'(k_1 a)\right)\left(\psi_l'(k_2 a) + t_{2l}\xi_l'(k_2 a)\right)} \\ f_{2l} = \dfrac{\mu}{\mu_1}\dfrac{1}{\frac{\eta}{\eta_2}\xi_l'(kb)\xi_l(k_2 b) - \xi_l(kb)\xi_l'(k_2 b)} \\ \qquad \cdot \dfrac{a_{2l}}{\left(A_{2l}\psi_l(k_1 a) - \psi_l'(k_1 a)\right)\left(\psi_l(k_2 a) + t_{2l}\xi_l(k_2 a)\right)} \end{cases}$$

These are the final expressions of the transmission problem. For a given excitation field $\boldsymbol{E}_{\mathrm{exc}}(\boldsymbol{r})$, we compute the expansion coefficients $a_{\tau n}$. The unknown coefficients $t_{\tau n}$, $r_{\tau n}$, $\alpha_{\tau n}$, and $f_{\tau n}$ are then found from the expressions above, and all fields can be evaluated.

3 Vertical electric elementary dipole excitation

The first simple excitation is a vertical electric elementary dipole located a distance $d \geq 0$ along the positive z-axis. The electric field of this excitation is proportional to

$$\boldsymbol{E}_{\mathrm{exc}}(\boldsymbol{r}) = \boldsymbol{u}_{2\mathrm{e}01}(k_1(\boldsymbol{r} - d\hat{\boldsymbol{z}}))$$

The corresponding magnetic field is

$$\boldsymbol{H}_{\mathrm{exc}}(\boldsymbol{r}) = \frac{1}{\mathrm{i}\eta_0\eta_1}\boldsymbol{u}_{1\mathrm{e}01}(k_1(\boldsymbol{r} - d\hat{\boldsymbol{z}}))$$

3.1 Determination of the expansion coefficients a_n

The determination of the expansion coefficients a_n for this excitation is now addressed.

The far-field amplitude of this excitation (no radome present) is [3, Sec: 4.1.3] and (A.1)

$$\boldsymbol{F}_0(\hat{\boldsymbol{r}}) = -\mathrm{i}\frac{\mathrm{e}^{-\mathrm{i}k_1 d\cos\theta}}{k_1}\boldsymbol{A}_{2\mathrm{e}01}(\hat{\boldsymbol{r}}) = \mathrm{i}\hat{\boldsymbol{\theta}}\sqrt{\frac{3}{8\pi}}\sin\theta\frac{\mathrm{e}^{-\mathrm{i}k_1 d\cos\theta}}{k_1} \tag{3.1}$$

The translation properties of the spherical vector waves easily determine the expansion coefficients a_n. We have, see (B.1)

$$\boldsymbol{u}_n(k_1(\boldsymbol{r}+\boldsymbol{d})) = \sum_{n'}\mathcal{R}_{nn'}(k_1\boldsymbol{d})\boldsymbol{u}_{n'}(k_1\boldsymbol{r}), \quad r > d \tag{3.2}$$

From this relation, the expansion coefficient $a_{\tau n} = \mathcal{R}_{2\mathrm{e}01,n}(-k_1 d\hat{\boldsymbol{z}}) = \mathcal{R}_{n,2\mathrm{e}01}(k_1 d\hat{\boldsymbol{z}})$ are readily found. The explicit expressions of the translation matrix $\mathcal{R}_{nn'}$ are given in Appendix B and [3, Appendix F.7]. More precisely, the translation matrix is

$$\mathcal{R}_{\tau\sigma ml,2\mathrm{e}01}(k_1 d\hat{\boldsymbol{z}}) = 2\delta_{\tau,2}\delta_{\sigma,\mathrm{e}}\delta_{m,0}C_{0l,01}(k_1 d, 0)$$

where the matrix $C_{ml,m'l'}$ is explicitly given in Appendix B and [3]

$$C_{0l,0l'}(d,\eta) = \frac{1}{4}\sum_{\lambda=|l-l'|}^{l+l'}\mathrm{i}^{l'-l+\lambda}(2\lambda+1)\sqrt{\frac{(2l+1)(2l'+1)}{l(l+1)l'(l'+1)}}$$
$$\times\begin{pmatrix} l & l' & \lambda \\ 0 & 0 & 0\end{pmatrix}^2 [l(l+1)+l'(l'+1)-\lambda(\lambda+1)]\,\mathrm{j}_\lambda(k_1 d)\mathrm{P}_\lambda(\cos\eta)$$

and where $\begin{pmatrix} \cdot & \cdot & \cdot \\ \cdot & \cdot & \cdot\end{pmatrix}$ denotes the Wigner 3-j symbol [2]. The explicit value of $a_{\tau l}$ is $(l = 1, 2, \ldots)$

$$a_{\tau n} = \delta_{\tau,2}\delta_{\sigma,\mathrm{e}}\delta_{m,0}\sum_{\lambda=l-1}^{l+1}\mathrm{i}^{1-l+\lambda}(2\lambda+1)\sqrt{\frac{3(2l+1)}{8l(l+1)}}$$
$$\times\begin{pmatrix} l & 1 & \lambda \\ 0 & 0 & 0\end{pmatrix}^2 [l(l+1)+2-\lambda(\lambda+1)]\,\mathrm{j}_\lambda(k_1 d)$$

To the lowest order in powers of $k_1 d$, we have

$$a_{\tau n} = \delta_{\tau,2}\delta_{\sigma,\mathrm{e}}\delta_{m,0}\delta_{l,1}3\begin{pmatrix} 1 & 1 & 0 \\ 0 & 0 & 0\end{pmatrix}^2 + O(k_1 d)$$
$$= \delta_{\tau,2}\delta_{\sigma,\mathrm{e}}\delta_{m,0}\delta_{l,1} + O(k_1 d), \qquad \text{as } k_1 d \to 0$$

If the dipole is located at the origin, the expansion coefficient for the vertical electric dipole is $a_{\tau n} = \delta_{\tau,2}\delta_{\sigma,\mathrm{e}}\delta_{m,0}\delta_{l,1}$.

3.2 Power transmission and far-field amplitude

The electric field in the far-field zone is [3, (7.31) on page 376]

$$\boldsymbol{E}_{\mathrm{t}}(\boldsymbol{r}) = \boldsymbol{F}(\hat{\boldsymbol{r}})\frac{\mathrm{e}^{\mathrm{i}kr}}{r}$$

where the far-field amplitude is

$$\boldsymbol{F}(\hat{\boldsymbol{r}}) = \frac{1}{\mathrm{i}k}\sum_{\substack{n\\ \tau=1,2}} f_{\tau n}\mathrm{i}^{-l+\tau-1}\boldsymbol{A}_{\tau n}(\hat{\boldsymbol{r}})$$

With the spherical geometry and the dipole excitation along the z axis, only $\tau = 2$, $\sigma = \mathrm{e}$, and $m = 0$ contribute, see (A.1).

$$\boldsymbol{F}(\hat{\boldsymbol{r}}) = -\hat{\boldsymbol{\theta}}\frac{\sin\theta}{k}\sum_{l=1}^{\infty}\mathrm{i}^{-l}\sqrt{\frac{2l+1}{4\pi l(l+1)}}\pi_l(\cos\theta)f_{2l}$$

The input power on a surface inside the radome that encloses the sources is [3, Eq. (7.18)]

$$P_{\mathrm{in}} = \frac{1}{2k_1^2\eta_0\eta_1}\sum_{l=1}^{\infty}\sum_{\tau=1}^{2}|a_{\tau l}|^2\left(1+\operatorname{Re} r_{\tau l}\right)$$

The radiated power on a surface that encloses the entire structure is

$$P_{\mathrm{rad}} = \frac{1}{2k^2\eta_0\eta}\sum_{l=1}^{\infty}\sum_{\tau=1}^{2}|f_{\tau l}|^2$$

The following quotient is of interest to compute:

$$\frac{P_{\mathrm{rad}}}{P_{\mathrm{in}}} = \frac{k_1^2\eta_1\sum_{l=1}^{\infty}\sum_{\tau=1}^{2}|f_{\tau l}|^2}{k^2\eta\sum_{l=1}^{\infty}\sum_{\tau=1}^{2}|a_{\tau l}|^2\left(1+\operatorname{Re} r_{\tau l}\right)} \tag{3.3}$$

Notice that this quotient, by energy conservation, for real-valued parameters has to be identical one. This is used in Section 3.5 as a tool of verification of the numerical precision of the code.

3.3 Near-field calculation

3.3.1 Internal field

The interior field excited by a vertical electric dipole located at $d\hat{\boldsymbol{z}}$ consists of two parts. The direct excitation is

$$\boldsymbol{E}_{\mathrm{exc}}(\boldsymbol{r}) = \boldsymbol{u}_{2\mathrm{e}01}(k_1(\boldsymbol{r}-d\hat{\boldsymbol{z}})) = -\frac{\xi_1'(k_1R)}{k_1R}\sqrt{\frac{3}{8\pi}}\sin\theta'\hat{\boldsymbol{\theta}}' + \frac{\xi_1(k_1R)}{k_1^2R^2}\sqrt{\frac{3}{2\pi}}\cos\theta'\hat{\boldsymbol{R}}$$

where $R = |\boldsymbol{r} - d\hat{\boldsymbol{z}}|$ and $\cos\theta' = (z-d)/R$ (distance and polar angle in the coordinate system located at the source, respectively). We also have

$$\xi_1(z) = -\mathrm{e}^{\mathrm{i}z}\left(1 + \frac{\mathrm{i}}{z}\right)$$

and

$$\begin{cases} \hat{\boldsymbol{R}} = \hat{\boldsymbol{r}}_\mathrm{c}\sin\theta' + \hat{\boldsymbol{z}}\cos\theta' \\ \hat{\boldsymbol{\theta}}' = \hat{\boldsymbol{r}}_\mathrm{c}\cos\theta' - \hat{\boldsymbol{z}}\sin\theta' \end{cases}$$

where $\hat{\boldsymbol{r}}_\mathrm{c} = (x\hat{\boldsymbol{x}} + y\hat{\boldsymbol{y}})/\sqrt{x^2+y^2}$. In terms of the global unit vectors $\hat{\boldsymbol{r}}_\mathrm{c}$ and $\hat{\boldsymbol{z}}$, we get

$$\boldsymbol{E}_\mathrm{exc}(\boldsymbol{r}) = \sqrt{\frac{3}{8\pi}}\Bigg\{-\frac{\xi_1'(k_1R)}{k_1R}\sin\theta'\left(\cos\theta'\hat{\boldsymbol{r}}_\mathrm{c} - \sin\theta'\hat{\boldsymbol{z}}\right) + 2\frac{\xi_1(k_1R)}{k_1^2R^2}\cos\theta'\left(\sin\theta'\hat{\boldsymbol{r}}_\mathrm{c} + \cos\theta'\hat{\boldsymbol{z}}\right)\Bigg\}$$

or in the units vectors evaluated at the origin

$$\boldsymbol{E}_\mathrm{exc}(\boldsymbol{r}) = \sqrt{\frac{3}{8\pi}}\Bigg\{-\frac{\xi_1'(k_1R)}{k_1R}\sin\theta'\left(\hat{\boldsymbol{r}}\sin(\theta-\theta') + \hat{\boldsymbol{\theta}}\cos(\theta-\theta')\right) + 2\frac{\xi_1(k_1R)}{k_1^2R^2}\cos\theta'\left(\hat{\boldsymbol{r}}\cos(\theta-\theta') - \hat{\boldsymbol{\theta}}\sin(\theta-\theta')\right)\Bigg\}$$

The corresponding magnetic field is

$$\boldsymbol{H}_\mathrm{exc}(\boldsymbol{r}) = \frac{1}{\mathrm{i}\eta_0\eta_1}\sqrt{\frac{3}{8\pi}}\frac{\xi_1(k_1R)}{k_1R}\sin\theta'\hat{\boldsymbol{\phi}}$$

In addition to this direct excitation, we have the reflected field

$$\boldsymbol{E}_\mathrm{ref}(\boldsymbol{r}) = \sum_{l=1}^{\infty} r_{2\mathrm{e}0l}a_{2\mathrm{e}0l}\left(\frac{\psi_l'(k_1r)}{k_1r}\boldsymbol{A}_{2\mathrm{e}0l}(\hat{\boldsymbol{r}}) + \sqrt{l(l+1)}\frac{\psi_l(k_1r)}{k_1^2r^2}\boldsymbol{A}_{3\mathrm{e}0l}(\hat{\boldsymbol{r}})\right)$$

and

$$\boldsymbol{H}_\mathrm{ref}(\boldsymbol{r}) = \frac{1}{\mathrm{i}\eta_0\eta_1}\sum_{l=1}^{\infty} r_{2\mathrm{e}0l}a_{2\mathrm{e}0l}\frac{\psi_l(k_1r)}{k_1r}\boldsymbol{A}_{1\mathrm{e}0l}(\hat{\boldsymbol{r}})$$

and the total internal field is

$$\boldsymbol{E}_\mathrm{int}(\boldsymbol{r}) = \boldsymbol{E}_\mathrm{exc}(\boldsymbol{r}) + \boldsymbol{E}_\mathrm{ref}(\boldsymbol{r}), \quad \boldsymbol{H}_\mathrm{int}(\boldsymbol{r}) = \boldsymbol{H}_\mathrm{exc}(\boldsymbol{r}) + \boldsymbol{H}_\mathrm{ref}(\boldsymbol{r})$$

The modulus of the local Poynting vector is an appropriate quantity to calculate (we here assume the magnetic field has only a $\tau = 1$ contribution, which is correct

for the vertical electric dipole excitation along the z axis).

$$\langle \boldsymbol{S}(t)\rangle(\boldsymbol{r}) = \frac{1}{2}\operatorname{Re}\left(\boldsymbol{E}_{\text{int}}(\boldsymbol{r}) \times \boldsymbol{H}^*_{\text{int}}(\boldsymbol{r})\right)$$
$$= \frac{1}{2}\operatorname{Re}\left(E_{r_\text{c}}(\boldsymbol{r})H^*_\phi(\boldsymbol{r})\right)\hat{\boldsymbol{z}} - \frac{1}{2}\operatorname{Re}\left(E_\text{z}(\boldsymbol{r})H^*_\phi(\boldsymbol{r})\right)\hat{\boldsymbol{r}}_\text{c}, \quad 0 \le r < a$$

where $E_{r_\text{c}} = \boldsymbol{E}_{\text{int}} \cdot \hat{\boldsymbol{r}}_\text{c}$, $E_\text{z} = \boldsymbol{E}_{\text{int}} \cdot \hat{\boldsymbol{z}}$, and $H_\phi = \boldsymbol{H}_{\text{int}} \cdot \hat{\boldsymbol{\phi}}$, and

$$|\langle \boldsymbol{S}(t)\rangle(\boldsymbol{r})|^2 = \frac{1}{4}\left\{\left|\operatorname{Re}\left(E_{r_\text{c}}(\boldsymbol{r})H^*_\phi(\boldsymbol{r})\right)\right|^2 + \left|\operatorname{Re}\left(E_\text{z}(\boldsymbol{r})H^*_\phi(\boldsymbol{r})\right)\right|^2\right\}, \quad 0 \le r < a$$

3.3.2 External field

The external field outside the spherical shell is ($r > b$)

$$\boldsymbol{E}_\text{t}(\boldsymbol{r}) = \sum_{l=1}^{\infty} f_{\text{2e0}l}\left(\frac{\xi_l'(kr)}{kr}\boldsymbol{A}_{\text{2e0}l}(\hat{\boldsymbol{r}}) + \sqrt{l(l+1)}\frac{\xi_l(kr)}{k^2r^2}\boldsymbol{A}_{\text{3e0}l}(\hat{\boldsymbol{r}})\right)$$

or more explicitly in terms of the functions $\pi_l(x) = \mathrm{P}_l'(x)$ and the Legendre polynomials $\mathrm{P}_l(x)$, see (A.1)

$$\boldsymbol{E}_\text{t}(\boldsymbol{r}) = \sum_{l=1}^{\infty} f_{\text{2e0}l}\sqrt{\frac{2l+1}{4\pi l(l+1)}}\left(-\hat{\boldsymbol{\theta}}\frac{\xi_l'(kr)}{kr}\pi_l(\cos\theta)\sin\theta + \hat{\boldsymbol{r}}l(l+1)\frac{\xi_l(kr)}{k^2r^2}\mathrm{P}_l(\cos\theta)\right)$$

In particular, for a dipole at the center of the spherical shell, $d = 0$, only $l = 1$ contributes, and the electric field is

$$\boldsymbol{E}_\text{t}(\boldsymbol{r}) = f_{\text{2e011}}\sqrt{\frac{3}{8\pi}}\left(-\hat{\boldsymbol{\theta}}\frac{\xi_1'(kr)}{kr}\sin\theta + 2\hat{\boldsymbol{r}}\frac{\xi_1(kr)}{k^2r^2}\cos\theta\right)$$

3.4 Illustrations

The results above are illustrated in this section.

3.4.1 Transmission

The transmission quotient in (3.3) is illustrated for a vertical dipole located at $0.5a\hat{\boldsymbol{z}}$ with interior material parameters $\epsilon_1/\epsilon = 1$ and $\mu_1/\mu = 1$. The material parameters of the lossy shell (thickness $t = \lambda/4$, where λ is the wavelength in the exterior medium) are $\epsilon_2/\epsilon = 3 + 6.4\mathrm{i}/ka$ and $\mu_2/\mu = 1$ (blue curve) and $\epsilon_2/\epsilon = 3 + 0.64\mathrm{i}/ka$ and $\mu_2/\mu = 1$ (red curve). The value of the imaginary part of ϵ_2 corresponds to a conductivity $\sigma = 0.017$ S/m and $\sigma = 0.0017$ S/m, respectively,[1] and the result is illustrated in Figure 3.

[1] The conductivities are constructed from a loss tangent of 0.01 and 0.001, respectively, at 10 GHz and $a = 1$ m.

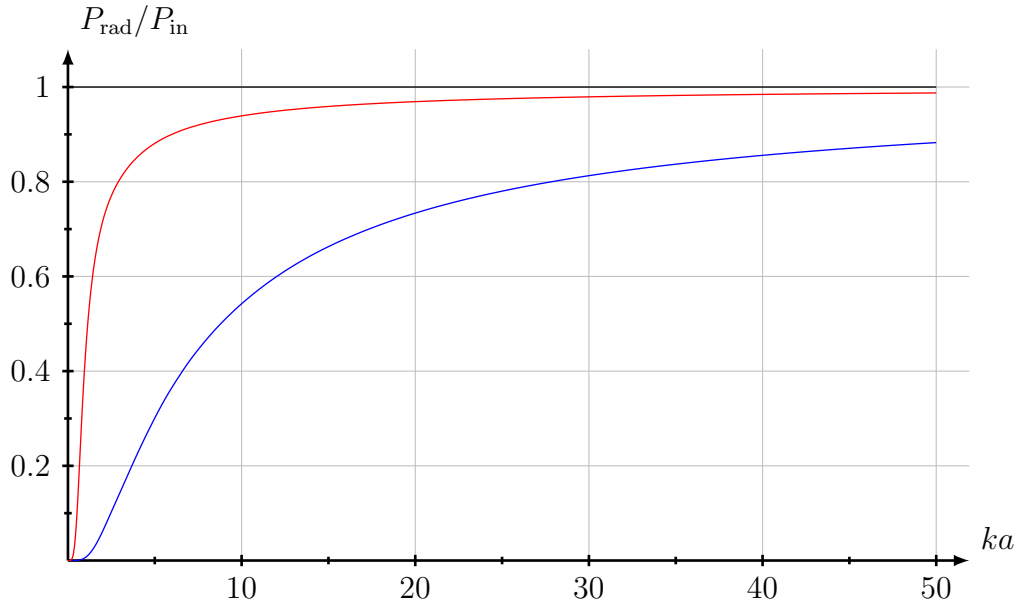

Figure 3: The quotient $P_{\rm rad}/P_{\rm in}$ for vertical electric dipole located at $0.5a\hat{\boldsymbol{z}}$ of a lossy spherical shell versus the electrical radius (scaled frequency) ka. The data used in the figure are given in the text.

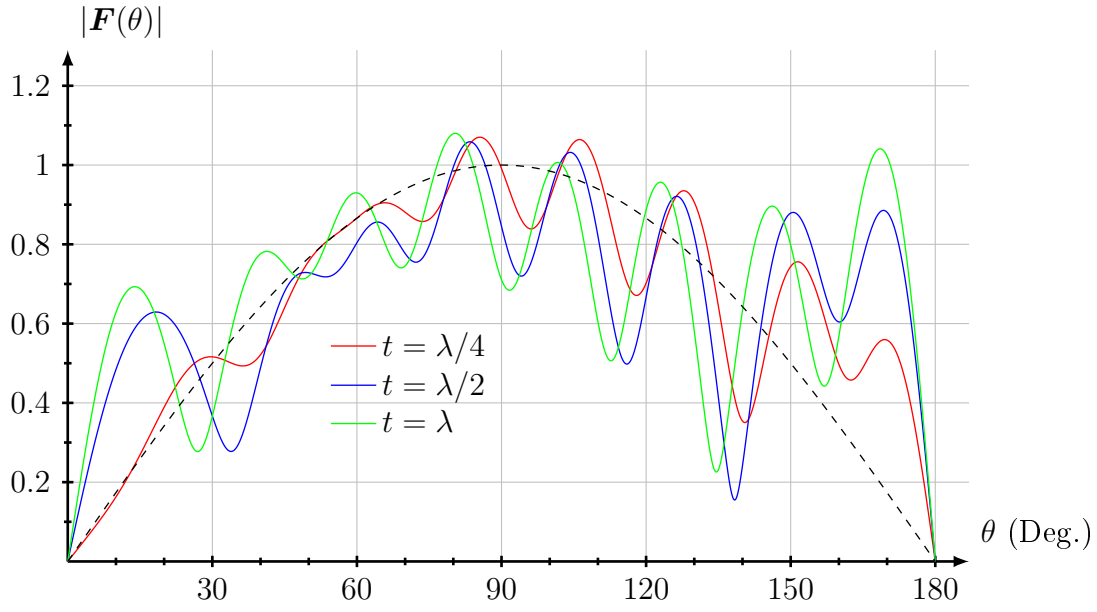

Figure 4: The far-field amplitude $|\boldsymbol{F}(\theta)|$ for a vertical electric dipole at $d\hat{\boldsymbol{z}} = 0.5a\hat{\boldsymbol{z}}$ versus θ for $a = 3\lambda$ at three different thicknesses t of the shell. The material data used in the figure are given in the text. The dashed curve is the far-field amplitude from the vertical electric dipole located at $d\hat{\boldsymbol{z}}$ without a lossy shell. The amplitudes are normalized to amplitude one at $\theta = 90^\circ$ in the absence of the lossy shell.

3.4.2 Far-field amplitude

We illustrate the absolute value of the far-field amplitude for a translated vertical dipole and a spherical lossy shell ($\epsilon_2/\epsilon = 3(1+0.01\mathrm{i})$, and $\mu_2/\mu = 1$) in Figures 4–6. The interior medium is lossless $\epsilon_1/\epsilon = 1$, $\mu_1/\mu = 1$. The electric size of the inner surface of the shell is $ka = 3\cdot 2\pi, 10\cdot 2\pi, 20\cdot 2\pi$ and the shell is $t = \lambda/4, \lambda/2, \lambda$ thick, respectively, where λ is the wavelength in the exterior medium.

3.4.3 Internal field

The modulus of the Poynting vector, $|\langle \boldsymbol{S}(t)\rangle\,(\boldsymbol{r})|$, is depicted in Figure 7 in the $y = 0$ plane in arbitrary units. The material parameters of the shell is $\epsilon_2/\epsilon = 3(1+0.01\mathrm{i})$, $\mu_2/\mu = 1$. The radius $a = 3\lambda$, and the shell is $t = \lambda/4$ thick, and $d/a = 0.5$, where λ is the wavelength in the exterior medium.

3.4.4 Near field

The modulus and the phase of tangential external electric field, $\hat{\boldsymbol{\theta}}\cdot\boldsymbol{E}_{\mathrm{t}}(\boldsymbol{r})$ — with and without spherical shell — at a fixed radial distance $r = 20\lambda$ versus θ are depicted in Figures 8 and 9, respectively. The interior medium is lossless $\epsilon_1/\epsilon = 1$, $\mu_1/\mu = 1$. The vertical electric dipole is translated along the z axis by a distance $d = 0.5a$. The material parameters of the shell is $\epsilon_2/\epsilon = 3(1+0.01\mathrm{i})$, $\mu_2/\mu = 1$. The radius $a = 10\lambda$, and the shell is $t = \lambda/4$ thick, where λ is the wavelength in the exterior medium.

In Figure 10, the absolute value of the total electric field, $|\boldsymbol{E}_{\mathrm{t}}(\boldsymbol{r})|$ — with and without spherical shell — is depicted. This field contains a small radial component, but the deviation from the corresponding absolute value of the tangential component, $|\hat{\boldsymbol{\theta}}\cdot\boldsymbol{E}_{\mathrm{t}}(\boldsymbol{r})|$, is small, see Figure 8. All other data are identical to Figures 8 and 9.

3.5 Verification

The numerical implementation is verified with two different methods, which are discussed in this section.

3.5.1 Power conservation

The first and most obvious way to verify the numerical implementation is to see how power conservation is satisfied. For real-valued material parameters, the expression

$$\frac{k_1^2\eta_1|f_{\tau l}|^2}{k^2\eta|a_{\tau l}|^2\,(1+\mathrm{Re}\,r_{\tau l})} - 1$$

should be zero for all indices $\tau = 1, 2$ and $l = 1, 2, \ldots$. Typical value for the computation presented here is 10^{-13}, and reflects the numerical precision of the Wronskian of the Riccati-Bessel functions.

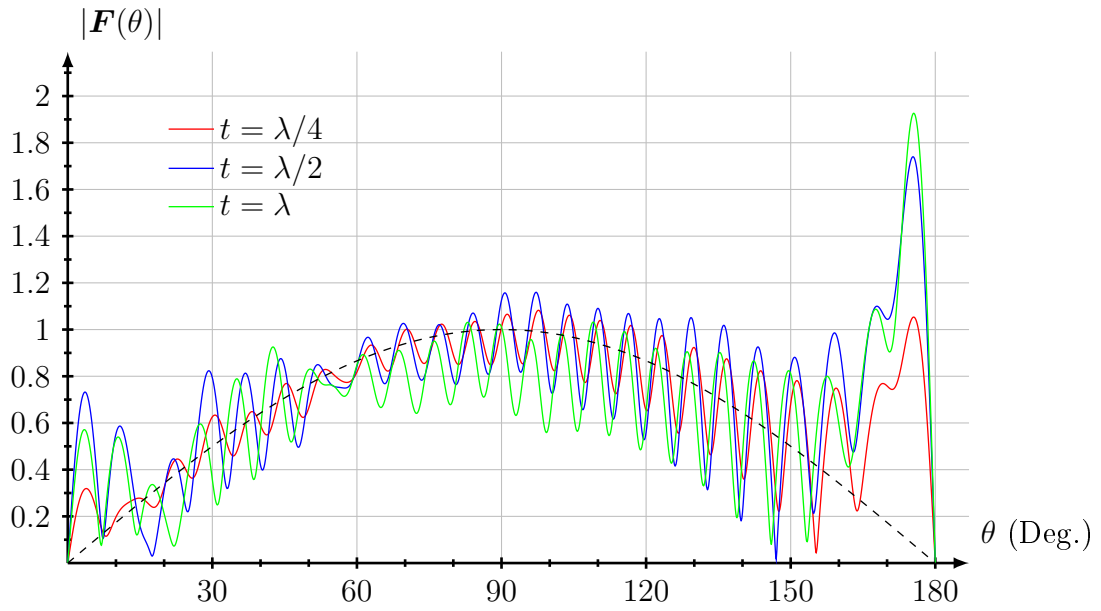

Figure 5: The far-field amplitude $|\boldsymbol{F}(\theta)|$ for a vertical electric dipole at $d\hat{\boldsymbol{z}} = 0.5a\hat{\boldsymbol{z}}$ versus θ for $a = 10\lambda$ at three different thicknesses t of the shell. All other data are identical to the ones given in Figure 4.

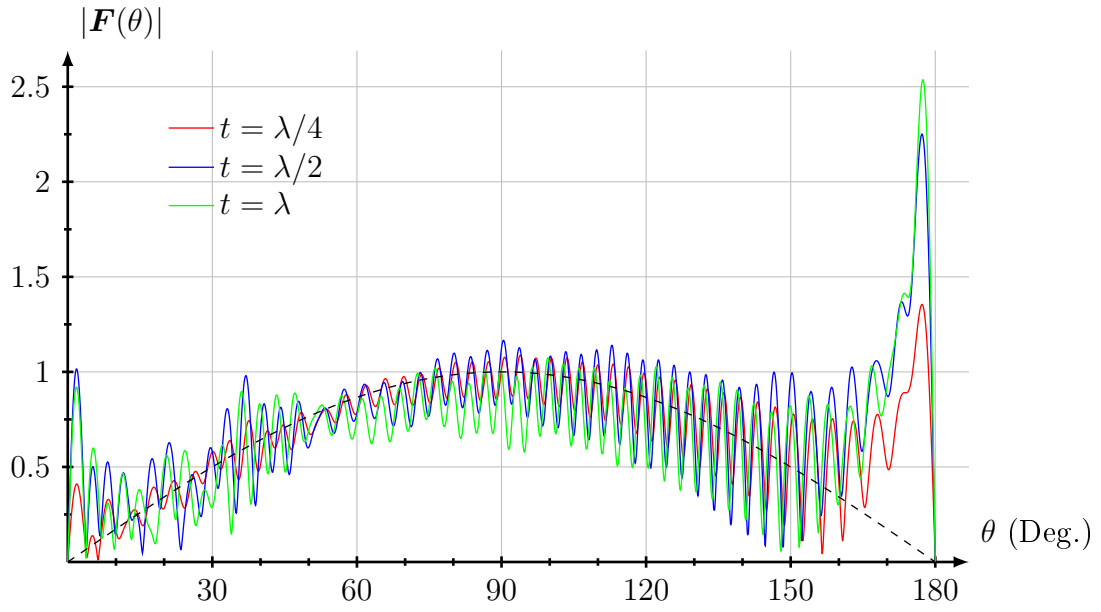

Figure 6: The far-field amplitude $|\boldsymbol{F}(\theta)|$ for a vertical electric dipole at $d\hat{\boldsymbol{z}} = 0.5a\hat{\boldsymbol{z}}$ versus θ for $a = 20\lambda$ at three different thicknesses t of the shell. All other data are identical to the ones given in Figure 4.

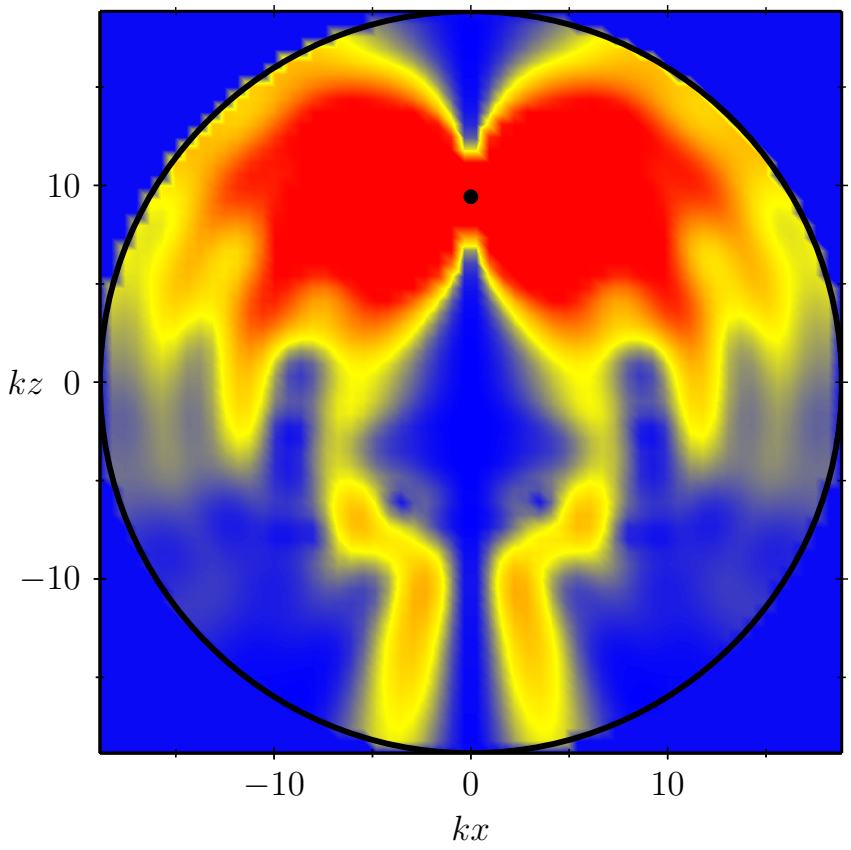

Figure 7: The modulus of the Poynting vector, $|\langle \boldsymbol{S}(t)\rangle(\boldsymbol{r})|$ inside the shell in the plane $y = 0$ in arbitrary units. The radius $a = 3\lambda$ and the remaining data of the figure are given in the text. Note that the infinite peak at the location of the dipole has been truncated. The location the vertical dipole is marked by a small black circle.

3.5.2 Shell of zero thickness

Another test is to let the radome have zero thickness and compare to the known expression of the excitation $\boldsymbol{F}_0(\hat{\boldsymbol{r}})$, see (3.1). In this test the material parameters inside and outside the radome have to be identical ($\epsilon_1/\epsilon = 1$, $\mu_1/\mu = 1$). The relative error is of the order 10^{-11}.

4 Circular disk with constant surface fields excitation (Huygens surface)

The vertical dipole excitation in Section 3 gives a first case of verification. Another excitation for verification purposes is a horizontal, circular disk of radius d with

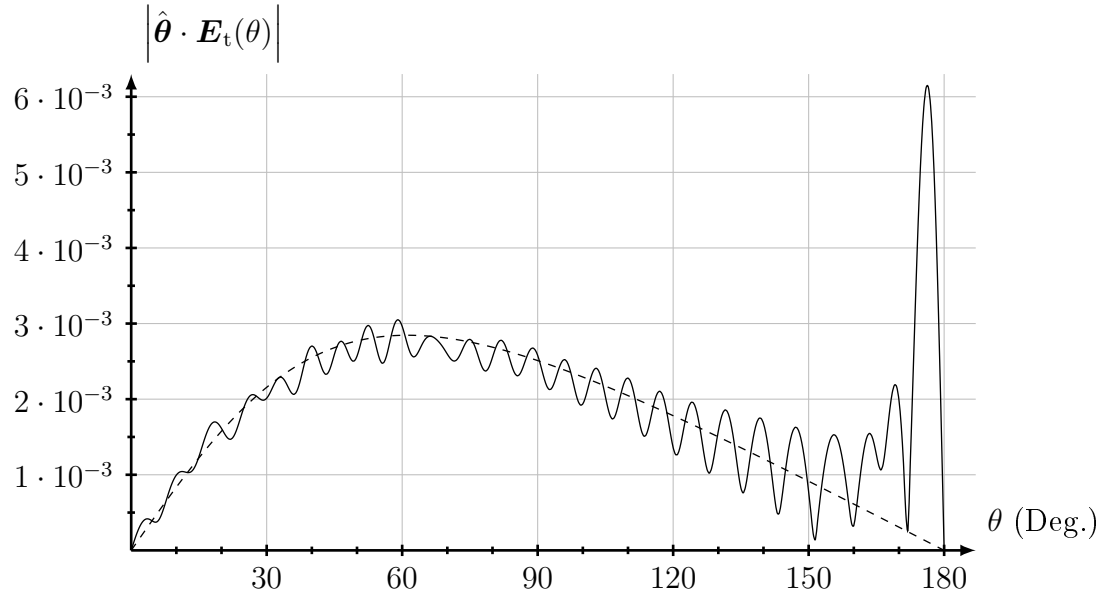

Figure 8: The absolute value of $\hat{\boldsymbol{\theta}} \cdot \boldsymbol{E}_{\mathrm{t}}(\theta)$ versus θ at a fixed radial distance $r = 20\lambda$ for a translated vertical electric dipole. Data of the spherical shell are given in the text. The dashed curve is the field without the spherical shell.

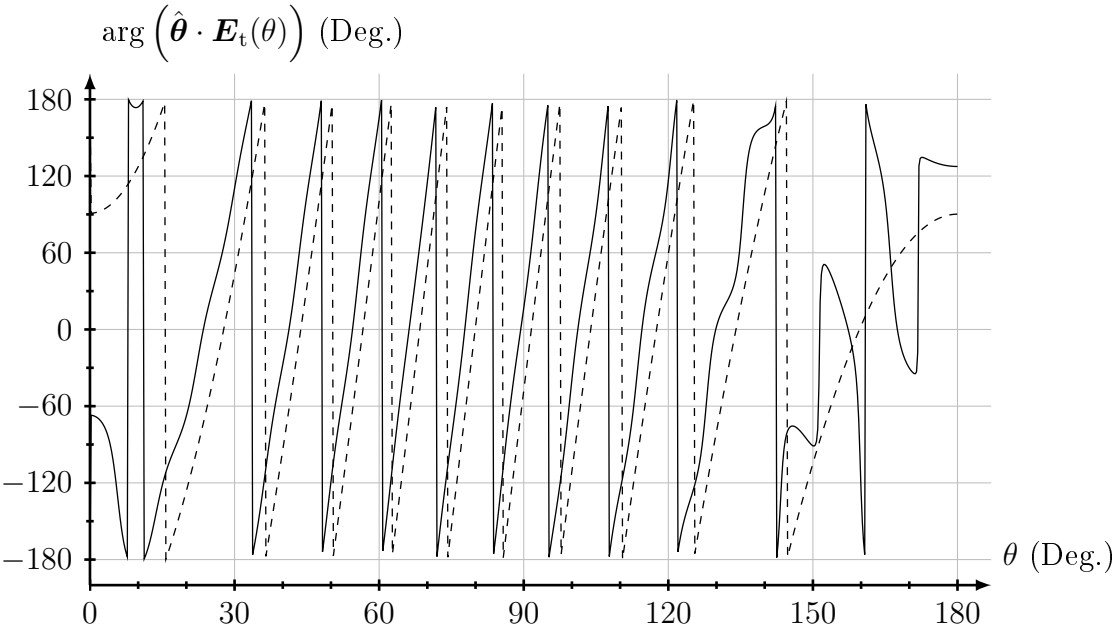

Figure 9: The phase of $\hat{\boldsymbol{\theta}} \cdot \boldsymbol{E}_{\mathrm{t}}(\theta)$ at a fixed radial distance $r = 20\lambda$ versus θ for a translated vertical electric dipole. Data of the spherical shell are given in the text. The dashed curve is the field without the spherical shell.

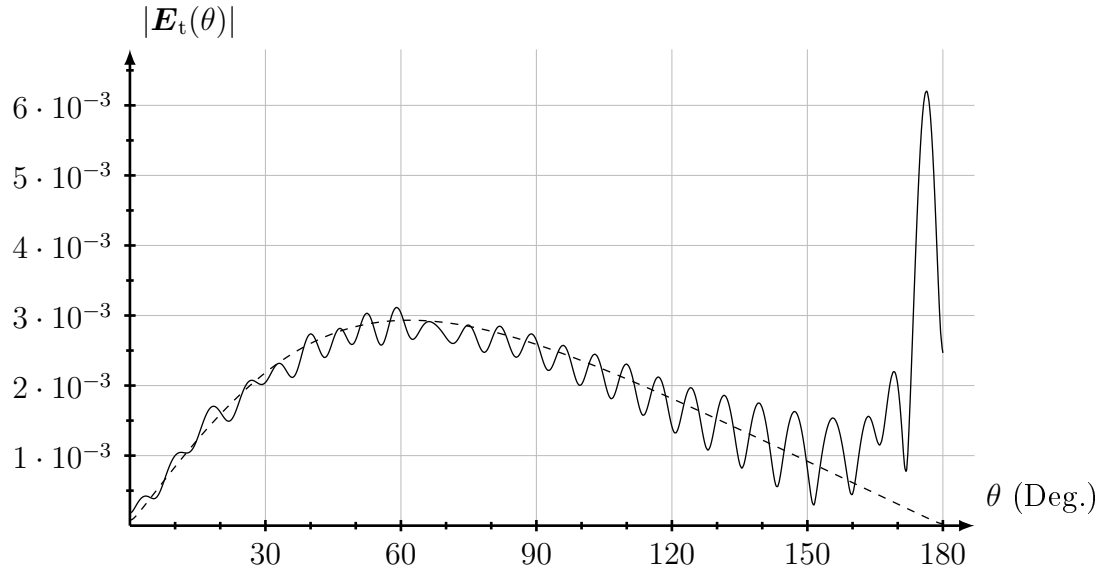

Figure 10: The absolute value of $\boldsymbol{E}_{\rm t}(\theta)$ versus θ at a fixed radial distance $r = 20\lambda$ for a translated vertical electric dipole. Data of the spherical shell are given in the text. The dashed curve is the field without the spherical shell.

fixed surface field distribution, see Figure 2. Assume

$$\boldsymbol{E}_{\rm exc}(\boldsymbol{r}) = E_0 {\rm H}(d - r_{\rm c})\hat{\boldsymbol{y}}, \qquad \boldsymbol{H}_{\rm exc}(\boldsymbol{r}) = -\frac{E_0}{\eta_0\eta_1}{\rm H}(d - r_{\rm c})\hat{\boldsymbol{x}}, \quad z = 0$$

where E_0 is a constant, complex-valued number and ${\rm H}(x)$ is the Heaviside function. This source on the disk radiates upwards in the $\hat{\boldsymbol{z}}$ direction (*cf.* plane wave excitation).

This excitation is of non-standard type. Usually, we require a specification of only one surface field to get a well-behaved solution to the problem. Here, we specify both the electric and the magnetic fields on the disk, which is acceptable in this case, since we do not require a boundary condition on the disk.

4.1 Determination of the expansion coefficients a_n

We now determine the expansion coefficients $a_{\tau n}$ for this disk excitation. To accomplish this, we use the far-field amplitude generated by this source.

The far-field amplitude is, see [3, (4.19) on page 198] ($\epsilon = \epsilon_1$ and $\mu = \mu_1$, and $\hat{\boldsymbol{\nu}} = \hat{\boldsymbol{z}}$)

$$\boldsymbol{F}_0(\hat{\boldsymbol{r}}) = \frac{{\rm i}k_1}{4\pi}\hat{\boldsymbol{r}} \times \iint_S \Big[\hat{\boldsymbol{z}} \times \boldsymbol{E}_{\rm exc}(\boldsymbol{r}') - \eta_0\eta_1 \hat{\boldsymbol{r}} \times (\hat{\boldsymbol{z}} \times \boldsymbol{H}_{\rm exc}(\boldsymbol{r}'))\Big] {\rm e}^{-{\rm i}k_1 \hat{\boldsymbol{r}}\cdot\boldsymbol{r}'} \, {\rm d}S'$$

$$= -\frac{{\rm i}k_1 E_0}{4\pi}\hat{\boldsymbol{r}} \times \int_0^{2\pi}\int_0^d [\hat{\boldsymbol{x}} - \hat{\boldsymbol{r}} \times \hat{\boldsymbol{y}}] \, {\rm e}^{-{\rm i}k_1 \hat{\boldsymbol{r}}\cdot\boldsymbol{r}_{\rm c}'} r_{\rm c}' \, {\rm d}r_{\rm c}' \, {\rm d}\phi'$$

where $\boldsymbol{r}_{\rm c}{}' = x'\hat{\boldsymbol{x}} + y'\hat{\boldsymbol{y}}$ and $r_{\rm c}' = |\boldsymbol{r}_{\rm c}{}'|$, and S is the upper surface of the disk. Simplification of the exponent gives

$$\boldsymbol{F}_0(\hat{\boldsymbol{r}}) = -\frac{\mathrm{i}k_1 E_0}{4\pi}\hat{\boldsymbol{r}} \times (\hat{\boldsymbol{x}} - \hat{\boldsymbol{r}} \times \hat{\boldsymbol{y}}) \int_0^{2\pi}\int_0^d \mathrm{e}^{-\mathrm{i}k_1 r_{\rm c}' \sin\theta\cos(\phi'-\phi)} r_{\rm c}' \,\mathrm{d}r_{\rm c}' \,\mathrm{d}\phi'$$

where $\hat{\boldsymbol{r}} = \hat{\boldsymbol{x}}\sin\theta\cos\phi + \hat{\boldsymbol{y}}\sin\theta\sin\phi + \hat{\boldsymbol{z}}\cos\theta$. Evaluation of the ϕ' integral gives

$$\begin{aligned}\boldsymbol{F}_0(\hat{\boldsymbol{r}}) &= \frac{\mathrm{i}k_1 E_0}{2}\hat{\boldsymbol{r}} \times (\hat{\boldsymbol{r}} \times \hat{\boldsymbol{y}} - \hat{\boldsymbol{x}}) \int_0^d r_{\rm c}' \mathrm{J}_0(k_1 r_{\rm c}' \sin\theta)\,\mathrm{d}r_{\rm c}' \\ &= \frac{\mathrm{i}dE_0 \mathrm{J}_1(k_1 d\sin\theta)}{2\sin\theta}\hat{\boldsymbol{r}} \times (\hat{\boldsymbol{r}} \times \hat{\boldsymbol{y}} - \hat{\boldsymbol{x}}) \\ &= \frac{k_1 d^2 E_0}{2\mathrm{i}} \frac{\mathrm{J}_1(k_1 d\sin\theta)}{k_1 d\sin\theta}(1+\cos\theta)\left(\hat{\boldsymbol{\theta}}\sin\phi + \hat{\boldsymbol{\phi}}\cos\phi\right)\end{aligned}$$

since $\int x\mathrm{J}_0(x)\,\mathrm{d}x = x\mathrm{J}_1(x)$. This is the exact expression of the far-field amplitude for the source analyzed in this section.

From the far-field amplitude, we construct the coefficients $a_{\tau n}$ that is the input to the computations for the transmission problem with the spherical shell in Section 2. We have, see [3, page 378]

$$\begin{aligned}a_{\tau n} &= \mathrm{i}^{l+2-\tau} k_1 \iint_\Omega \boldsymbol{A}_{\tau n}(\hat{\boldsymbol{r}}) \cdot \boldsymbol{F}_0(\hat{\boldsymbol{r}})\,\mathrm{d}\Omega \\ &= \mathrm{i}^{l+1-\tau} \iint_\Omega \boldsymbol{A}_{\tau n}(\hat{\boldsymbol{r}}) \cdot \left(\hat{\boldsymbol{\theta}}\sin\phi + \hat{\boldsymbol{\phi}}\cos\phi\right) h(\theta)\,\mathrm{d}\Omega\end{aligned}$$

where

$$h(\theta) = \frac{k_1 dE_0 \mathrm{J}_1(k_1 d\sin\theta)}{2\sin\theta}(1+\cos\theta)$$

We focus on the integration in the azimuthal angle ϕ. The following integrals are of interest:

$$\int_0^{2\pi} \cos\phi \begin{Bmatrix}\cos m\phi \\ \sin m\phi\end{Bmatrix} \mathrm{d}\phi = \pi\delta_{m1}\begin{Bmatrix}1\\0\end{Bmatrix}$$

and

$$\int_0^{2\pi} \sin\phi \begin{Bmatrix}\cos m\phi \\ \sin m\phi\end{Bmatrix} \mathrm{d}\phi = \pi\delta_{m1}\begin{Bmatrix}0\\1\end{Bmatrix}$$

and as consequence, only $m = 1$ survives in the integration of the azimuthal angle ϕ. The definition of the vector spherical harmonics implies, see (A.2) or in [3, (C.13) on page 632]

$$a_{1n} = -\frac{\delta_{\sigma\mathrm{e}}\delta_{m1}\mathrm{i}^l \pi\sqrt{2l+1}}{\sqrt{2\pi}l(l+1)} \int_0^\pi (\pi_l(\cos\theta) + \tau_l(\cos\theta))\, h(\theta)\,\sin\theta\,\mathrm{d}\theta$$

and

$$a_{2n} = \frac{\delta_{\sigma\mathrm{o}}\delta_{m1}\mathrm{i}^{l-1} \pi\sqrt{2l+1}}{\sqrt{2\pi}l(l+1)} \int_0^\pi (\pi_l(\cos\theta) + \tau_l(\cos\theta))\, h(\theta)\,\sin\theta\,\mathrm{d}\theta$$

where

$$\begin{cases} \pi_l(x) = \mathrm{P}_l'(x) \\ \tau_l(x) = l(l+1)\mathrm{P}_l(x) - x\mathrm{P}_l'(x) = l^2\mathrm{P}_l(x) - \pi_{l-1}(x) \end{cases}$$

The combination of Legendre polynomials in the integrand has the form

$$(\pi_l(x) + \tau_l(x))\,(1+x) = \frac{l^2(l+1)}{2l+1}\mathrm{P}_{l+1}(x) + l(l+1)\mathrm{P}_l(x) + \frac{l(l+1)^2}{2l+1}\mathrm{P}_{l-1}(x)$$

To evaluate the coefficients $a_{\tau n}$, we need to find

$$I_l(z) = \int_0^\pi \frac{\mathrm{J}_1(z\sin\theta)}{z\sin\theta}\mathrm{P}_l(\cos\theta)\,\sin\theta\,\mathrm{d}\theta$$

Notice that $I_l(z) = 0$, if l is an odd, positive integer. Fortunately, these integral have a closed form solution. A proof of this integral is given in Appendix C. In terms of the integral $I_l(z)$, the expansion coefficients are

$$a_{1n} = -\frac{\delta_{\sigma\mathrm{e}}\delta_{m1}\mathrm{i}^l\pi(k_1d)^2E_0}{2\sqrt{2\pi}\sqrt{2l+1}}\left\{lI_{l+1}(k_1d) + (2l+1)I_l(k_1d) + (l+1)I_{l-1}(k_1d)\right\}$$

and

$$a_{2n} = \frac{\delta_{\sigma\mathrm{o}}\delta_{m1}\mathrm{i}^{l-1}\pi(k_1d)^2E_0}{2\sqrt{2\pi}\sqrt{2l+1}}\left\{lI_{l+1}(k_1d) + (2l+1)I_l(k_1d) + (l+1)I_{l-1}(k_1d)\right\}$$

The far-field amplitude is then recovered in terms of an expansion in vector spherical harmonics [3]

$$\boldsymbol{F}_0(\hat{\boldsymbol{r}}) = \frac{1}{\mathrm{i}k_1}\sum_{\substack{n\\ \tau=1,2}} a_{\tau n}\mathrm{i}^{-l+\tau-1}\boldsymbol{A}_{\tau n}(\hat{\boldsymbol{r}})$$

or more explicitly

$$\begin{aligned}\boldsymbol{F}_0(\hat{\boldsymbol{r}}) = {} & \frac{(k_1d)^2E_0}{4\mathrm{i}k_1}\left(\hat{\boldsymbol{\theta}}\sin\phi + \hat{\boldsymbol{\phi}}\cos\phi\right) \\ & \times\sum_{l=1}^{\infty}\frac{\left(lI_{l+1}(k_1d) + (2l+1)I_l(k_1d) + (l+1)I_{l-1}(k_1d)\right)\left(\pi_l(\cos\theta) + \tau_l(\cos\theta)\right)}{l(l+1)}\end{aligned}$$

4.2 Power transmission and far-field amplitude

The electric field in the far-field zone is [3, (7.31) on page 376]

$$\boldsymbol{E}_\mathrm{t}(\boldsymbol{r}) = \boldsymbol{F}(\hat{\boldsymbol{r}})\frac{\mathrm{e}^{\mathrm{i}kr}}{r}$$

where the far-field amplitude is

$$\boldsymbol{F}(\hat{\boldsymbol{r}}) = \frac{1}{\mathrm{i}k}\sum_{\substack{n\\ \tau=1,2}} f_{\tau n}\mathrm{i}^{-l+\tau-1}\boldsymbol{A}_{\tau n}(\hat{\boldsymbol{r}})$$

With the disk geometry of this section, only $m = 1$ contributes in the sum, see (A.2).

We proceed as in Section 3.2, but now the explicit form of the vector spherical harmonics for $m = 1$. Again, the quotient of the radiated and the incident power is of interest to compute

$$\frac{P_{\rm rad}}{P_{\rm in}} = \frac{k_1^2\eta_1 \sum_{l=1}^{\infty}\sum_{\tau=1}^{2} |f_{\tau l}|^2}{k^2\eta \sum_{l=1}^{\infty}\sum_{\tau=1}^{2} |a_{\tau l}|^2 \left(1 + \mathrm{Re}\, r_{\tau l}\right)} \tag{4.1}$$

Notice that this quotient, by energy conservation, for real-valued parameters has to be identical one. This is used in Section 4.4 as a tool of verification of the numerical precision of the code.

4.3 Illustrations

The results above are illustrated in this section.

4.3.1 Transmission

The transmission quotient in (4.1) is illustrated in Figure 11 for a circular disk with constant surface field excitation. The disk is centered at the origin with interior material parameters $\epsilon_1/\epsilon = 1$ and $\mu_1/\mu = 1$. The radius of the disk is $d = 0.5a$. The material parameters of the lossy shell (thickness $t = \lambda/4$, where λ is the wavelength in the exterior medium) are $\epsilon_2/\epsilon = 3 + 6.4\mathrm{i}/ka$ and $\mu_2/\mu = 1$ (blue curve) and $\epsilon_2/\epsilon = 3 + 0.64\mathrm{i}/ka$ and $\mu_2/\mu = 1$ (red curve). The value of the imaginary part of ϵ_2 corresponds to a conductivity $\sigma = 0.017$ S/m and $\sigma = 0.0017$ S/m, respectively. The values differ very little from the result for the translated electric dipole in Figure 3.

4.3.2 Far-field amplitude

The absolute value of the far-field amplitude for a circular disk of radius $d = 0.5a$ is illustrated for a spherical lossy shell ($\epsilon_2/\epsilon = 3(1 + 0.01\mathrm{i})$, and $\mu_2/\mu = 1$) in Figures 12–14. The interior medium is lossless $\epsilon_1/\epsilon = 1$, $\mu_1/\mu = 1$. The electric size of the inner surface of the shell is $ka = 3 \cdot 2\pi, 10 \cdot 2\pi, 20 \cdot 2\pi$ and the shell is $t = \lambda/4, \lambda/2, \lambda$ thick, respectively, where λ is the wavelength in the exterior medium.

4.4 Verifications

The numerical implementation is verified with two different methods, which are discussed in this section.

4.4.1 Power conservation

We verify the numerical implementation by how well power conservation is satisfied. For real-valued material parameters, the expression

$$1 - \frac{k_1^2\eta_1 \sum_{l=1}^{\infty}\sum_{\tau=1}^{2} |f_{\tau l}|^2}{k^2\eta \sum_{l=1}^{\infty}\sum_{\tau=1}^{2} |a_{\tau l}|^2 \left(1 + \mathrm{Re}\, r_{\tau l}\right)}$$

should be zero. Typical value for the computation presented here is 10^{-13}.

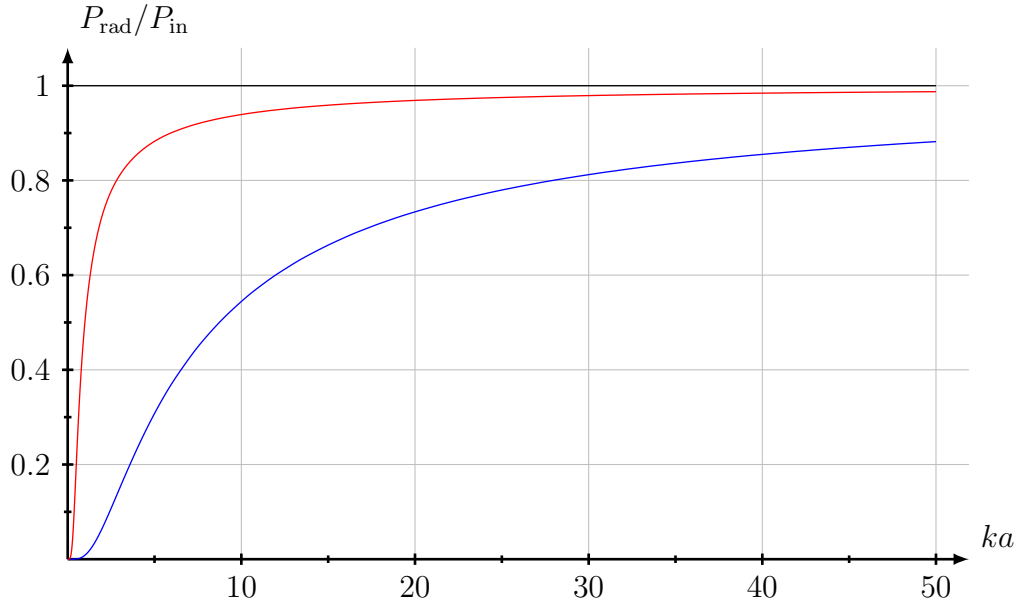

Figure 11: The quotient $P_{\rm rad}/P_{\rm in}$ for circular disk centered at the origin of a lossy spherical shell versus the electrical radius (scaled frequency) ka. The data used in the figure are given in the text.

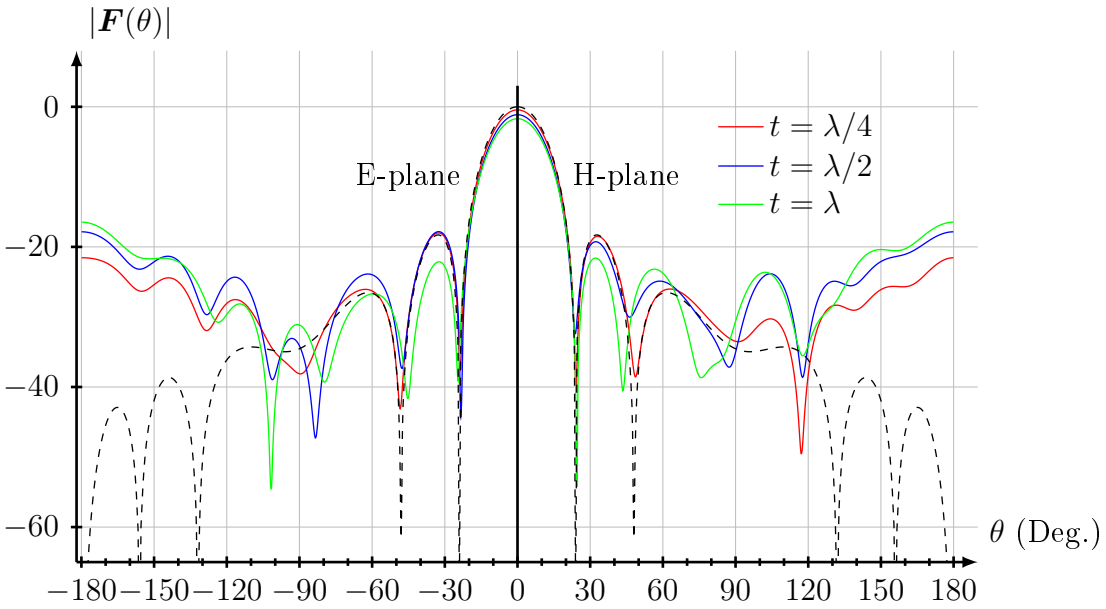

Figure 12: The far field amplitude $|\boldsymbol{F}(\theta)|$ for a circular disk of radius $d = 0.5a$ versus θ for $a = 3\lambda$ at three different thicknesses t of the shell. The material data used in the figure are given in the text. The dashed curve is the far-field amplitude from the circular disk located at the origin without a lossy shell. The amplitudes are normalized to amplitude one at $\theta = 0^\circ$ in the absence of the lossy shell.

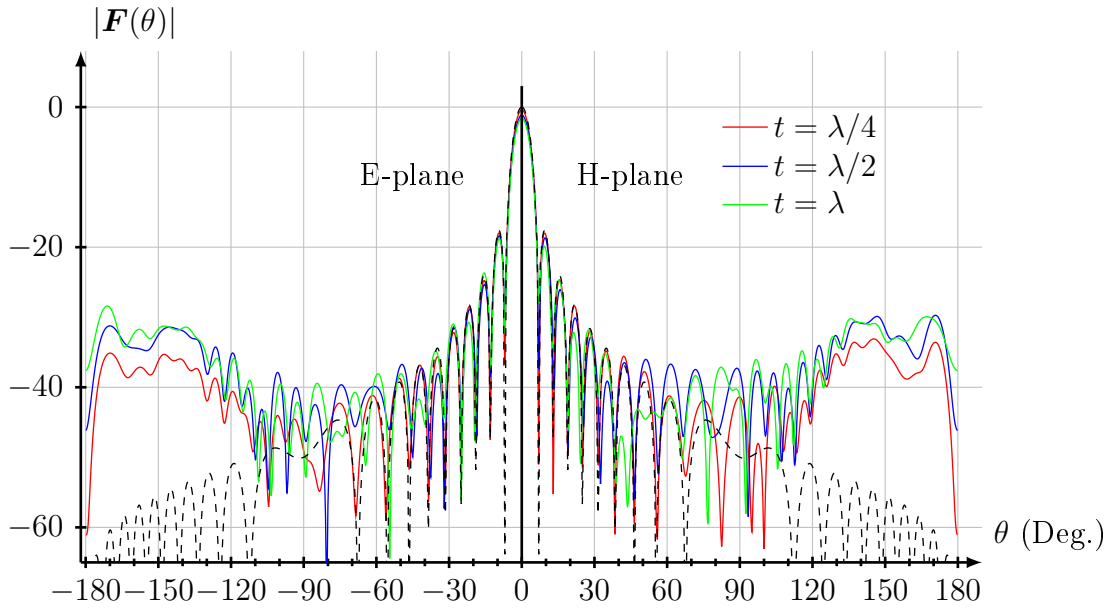

Figure 13: The far-field amplitude $|\boldsymbol{F}(\theta)|$ for a circular disk of radius $d = 0.5a$ versus θ for $a = 10\lambda$ at three different thicknesses t of the shell. All other data are identical to the ones given in Figure 12.

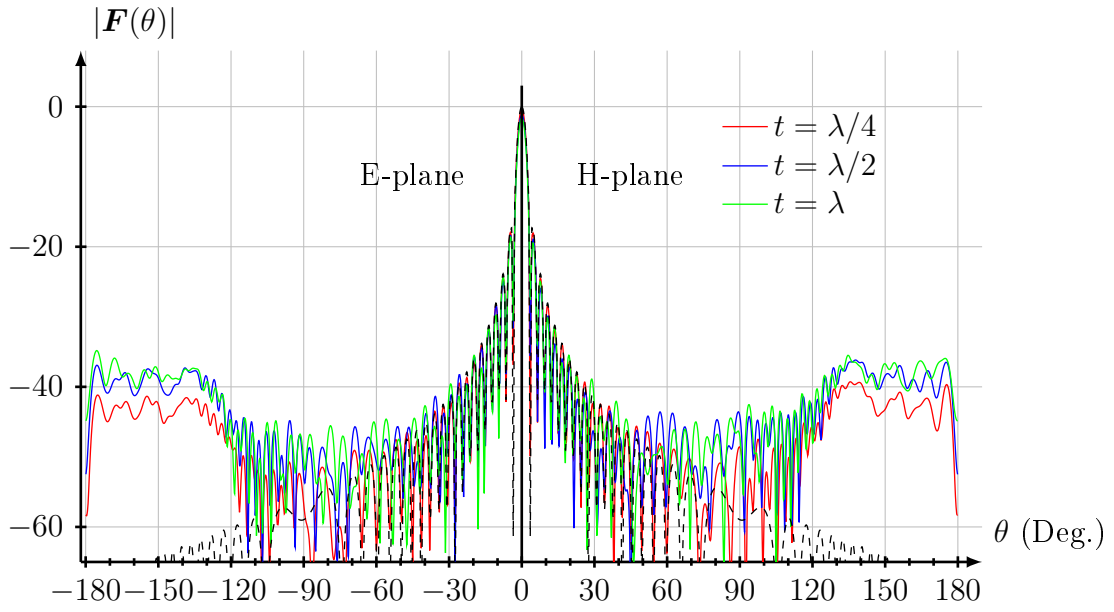

Figure 14: The far-field amplitude $|\boldsymbol{F}(\theta)|$ for a circular disk of radius $d = 0.5a$ versus θ for $a = 20\lambda$ at three different thicknesses t of the shell. All other data are identical to the ones given in Figure 12.

4.4.2 Shell of zero thickness

If the shell is of zero thickness or if the material parameters of the shell are identical to the ones inside and outside the spherical shell (air radome), the far-field amplitude should be identical to the result without the shell. This result is satisfied with an error less than 10^{-11}.

5 Conclusions

The transmission problem with a spherical, dielectric shell, excited by a source inside the shell, has been examined. Two different excitations have been analyzed — a displaced electric dipole and a circular disk with specific values. This problem has a closed form solution as a sum of spherical vector waves, where the expansion coefficients can be obtained with high accuracy. All integral are evaluated with machine precision, which guarantees a solution that can serve as a verification tool for methods with approximations.

Several generalizations of the transmission problem treated in this paper are relevant, and they will be addressed in a future study. In particular, the source configuration, which in this paper has no support and floats in free space, is usually supported or backed up with a PEC structure. This more complex transmission problem with a supporting structure (*i.e.*, a scatterer inside the spherical shell) models the interaction effects between the source and the radome (the spherical shell) in a more accurate way.

6 Acknowledgement

The analysis presented in this paper was made possible by a generous support by Applied Composites AB — a radome design and manufacturer in the Saab Group. This support is gratefully acknowledged.

Appendix A Spherical vector waves

The vector spherical harmonics are defined as [1, 3]

$$\begin{cases} \boldsymbol{A}_{1n}(\hat{\boldsymbol{r}}) = \dfrac{1}{\sqrt{l(l+1)}} \nabla \times (\boldsymbol{r} Y_n(\hat{\boldsymbol{r}})) = \dfrac{1}{\sqrt{l(l+1)}} \nabla \mathrm{Y}_n(\hat{\boldsymbol{r}}) \times \boldsymbol{r} \\ \boldsymbol{A}_{2n}(\hat{\boldsymbol{r}}) = \dfrac{1}{\sqrt{l(l+1)}} r \nabla \mathrm{Y}_n(\hat{\boldsymbol{r}}) \\ \boldsymbol{A}_{3n}(\hat{\boldsymbol{r}}) = \hat{\boldsymbol{r}} \mathrm{Y}_n(\hat{\boldsymbol{r}}) \end{cases}$$

where the spherical harmonics are denoted by $\mathrm{Y}_n(\hat{\boldsymbol{r}})$. The index n is a multi-index for the integer indices $l = 1, 2, 3, \ldots$, $m = 0, 1, \ldots, l$, and $\sigma =$ e,o (even and odd

in the azimuthal angle).[2] From these definitions, we see that the first two vector spherical harmonics, $\boldsymbol{A}_{1n}(\hat{\boldsymbol{r}})$ and $\boldsymbol{A}_{2n}(\hat{\boldsymbol{r}})$, are tangential to the unit sphere Ω in $\mathbb{R}^3$ and they are related as

$$\begin{cases} \hat{\boldsymbol{r}} \times \boldsymbol{A}_{1n}(\hat{\boldsymbol{r}}) = \boldsymbol{A}_{2n}(\hat{\boldsymbol{r}}) \\ \hat{\boldsymbol{r}} \times \boldsymbol{A}_{2n}(\hat{\boldsymbol{r}}) = -\boldsymbol{A}_{1n}(\hat{\boldsymbol{r}}) \end{cases}$$

The vector spherical harmonics form an orthonormal set over the unit sphere Ω in $\mathbb{R}^3$, *i.e.*,

$$\iint_{\Omega} \boldsymbol{A}_{\tau n}(\hat{\boldsymbol{r}}) \cdot \boldsymbol{A}_{\tau' n'}(\hat{\boldsymbol{r}}) \, \mathrm{d}\Omega = \delta_{nn'}\delta_{\tau\tau'}$$

where $\mathrm{d}\Omega$ is the surface measure on the unit sphere Ω.

The vector spherical harmonics for $m = 0$ for a general l index are [3, p. 632]

$$\begin{cases} \boldsymbol{A}_{1\sigma 0l}(\hat{\boldsymbol{r}}) = \hat{\boldsymbol{\phi}}\delta_{\sigma \mathrm{e}} \sqrt{\dfrac{2l+1}{4\pi l(l+1)}} \pi_l(\cos\theta)\sin\theta \\ \boldsymbol{A}_{2\sigma 0l}(\hat{\boldsymbol{r}}) = -\hat{\boldsymbol{\theta}}\delta_{\sigma \mathrm{e}} \sqrt{\dfrac{2l+1}{4\pi l(l+1)}} \pi_l(\cos\theta)\sin\theta \\ \boldsymbol{A}_{3\sigma 0l}(\hat{\boldsymbol{r}}) = \hat{\boldsymbol{r}}\delta_{\sigma \mathrm{e}} \sqrt{\dfrac{2l+1}{4\pi}} \mathrm{P}_l(\cos\theta) \end{cases} \tag{A.1}$$

where $\pi_l(x) = \mathrm{P}_l'(x)$ ($\pi_1(x) = 1$). The explicit form of the vector spherical harmonics for $m = 1$ is

$$\begin{cases} \boldsymbol{A}_{1\sigma 1l}(\hat{\boldsymbol{r}}) = \dfrac{\sqrt{2l+1}}{\sqrt{2\pi} l(l+1)} \left(\hat{\boldsymbol{\theta}} \pi_l(\cos\theta) \begin{Bmatrix} -\sin\phi \\ \cos\phi \end{Bmatrix} - \hat{\boldsymbol{\phi}} \tau_l(\cos\theta) \begin{Bmatrix} \cos\phi \\ \sin\phi \end{Bmatrix} \right) \\ \boldsymbol{A}_{2\sigma 1l}(\hat{\boldsymbol{r}}) = \dfrac{\sqrt{2l+1}}{\sqrt{2\pi} l(l+1)} \left(\hat{\boldsymbol{\phi}} \pi_l(\cos\theta) \begin{Bmatrix} -\sin\phi \\ \cos\phi \end{Bmatrix} + \hat{\boldsymbol{\theta}} \tau_l(\cos\theta) \begin{Bmatrix} \cos\phi \\ \sin\phi \end{Bmatrix} \right) \\ \boldsymbol{A}_{3\sigma 1l}(\hat{\boldsymbol{r}}) = \sqrt{\dfrac{2l+1}{2\pi l(l+1)}} \hat{\boldsymbol{r}} \sin\theta \pi_l(\cos\theta) \begin{Bmatrix} \cos\phi \\ \sin\phi \end{Bmatrix} \end{cases} \tag{A.2}$$

where

$$\begin{cases} \pi_l(x) = \mathrm{P}_l'(x) \\ \tau_l(x) = l(l+1)\mathrm{P}_l(x) - x\mathrm{P}_l'(x) = l^2 \mathrm{P}_l(x) - \pi_{l-1}(x) \end{cases}$$

The radiating solutions to the Maxwell equations in the exterior medium are defined as (outgoing spherical vector waves, $\boldsymbol{u}_{\tau n}(k\boldsymbol{r})$)

$$\begin{cases} \boldsymbol{u}_{1n}(k\boldsymbol{r}) = \dfrac{\xi_l(kr)}{kr} \boldsymbol{A}_{1n}(\hat{\boldsymbol{r}}) \\ \boldsymbol{u}_{2n}(k\boldsymbol{r}) = \dfrac{1}{k} \nabla \times \left(\dfrac{\xi_l(kr)}{kr} \boldsymbol{A}_{1n}(\hat{\boldsymbol{r}}) \right) \end{cases}$$

[2] The index set at several places in this paper also denotes a four index set, and includes the τ index. That is, the index n can denote $n = \{\sigma, l, m\}$ or $n = \{\tau, \sigma, l, m\}$.

Here, we use the Riccati-Bessel functions $\xi_l(x) = x\mathrm{h}_l^{(1)}(x)$, where $\mathrm{h}_l^{(1)}(x)$ is the spherical Hankel function of the first kind [4]. These vector waves satisfy

$$\nabla \times (\nabla \times \boldsymbol{u}_{\tau n}(k\boldsymbol{r})) - k^2 \boldsymbol{u}_{\tau n}(k\boldsymbol{r}) = \boldsymbol{0}, \qquad \tau = 1, 2$$

and they also satisfy the Silver-Müller radiation condition [3]. Another representation of the definition of the vector waves is

$$\begin{cases} \boldsymbol{u}_{1n}(k\boldsymbol{r}) = \dfrac{\xi_l(kr)}{kr} \boldsymbol{A}_{1n}(\hat{\boldsymbol{r}}) \\ \boldsymbol{u}_{2n}(k\boldsymbol{r}) = \dfrac{\xi_l'(kr)}{kr} \boldsymbol{A}_{2n}(\hat{\boldsymbol{r}}) + \sqrt{l(l+1)} \dfrac{\xi_l(kr)}{(kr)^2} \boldsymbol{A}_{3n}(\hat{\boldsymbol{r}}) \end{cases}$$

A simple consequence of these definitions is

$$\begin{cases} \boldsymbol{u}_{1n}(k\boldsymbol{r}) = \dfrac{1}{k} \nabla \times \boldsymbol{u}_{2n}(k\boldsymbol{r}) \\ \boldsymbol{u}_{2n}(k\boldsymbol{r}) = \dfrac{1}{k} \nabla \times \boldsymbol{u}_{1n}(k\boldsymbol{r}). \end{cases}$$

In a similar way, the regular spherical vector waves, $\boldsymbol{v}_{\tau n}(k\boldsymbol{r})$, are defined [1].

$$\begin{cases} \boldsymbol{v}_{1n}(k\boldsymbol{r}) = \dfrac{\psi_l(kr)}{kr} \boldsymbol{A}_{1n}(\hat{\boldsymbol{r}}) \\ \boldsymbol{v}_{2n}(k\boldsymbol{r}) = \dfrac{\psi_l'(kr)}{kr} \boldsymbol{A}_{2n}(\hat{\boldsymbol{r}}) + \sqrt{l(l+1)} \dfrac{\psi_l(kr)}{(kr)^2} \boldsymbol{A}_{3n}(\hat{\boldsymbol{r}}) \end{cases}$$

where the Riccati-Bessel functions $\psi_l(x) = x\mathrm{j}_l(x)$, where $\mathrm{j}_l(x)$ is the spherical Bessel function of the first kind [4].

Appendix B The translation matrices

The translation properties of the spherical vector waves are well know, and we refer to, *e.g.*, [1] for details.

Let $\boldsymbol{r}' = \boldsymbol{r} + \boldsymbol{d}$, see Figure 15. Then

$$\begin{cases} \boldsymbol{v}_n(k\boldsymbol{r}') = \sum_{n'} \mathcal{R}_{nn'}(k\boldsymbol{d}) \boldsymbol{v}_{n'}(k\boldsymbol{r}), & \text{for all } \boldsymbol{d} \\ \boldsymbol{u}_n(k\boldsymbol{r}') = \sum_{n'} \mathcal{R}_{nn'}(k\boldsymbol{d}) \boldsymbol{u}_{n'}(k\boldsymbol{r}), & r > d \\ \boldsymbol{u}_n(k\boldsymbol{r}') = \sum_{n'} \mathcal{P}_{nn'}(k\boldsymbol{d}) \boldsymbol{v}_{n'}(k\boldsymbol{r}), & r < d \end{cases} \tag{B.1}$$

Translation in the opposite direction is identical to the transpose of the translation matrices, *i.e.*,

$$\mathcal{R}^{\mathrm{t}}(k\boldsymbol{d}) = \mathcal{R}(-k\boldsymbol{d}), \quad \mathcal{P}^{\mathrm{t}}(k\boldsymbol{d}) = \mathcal{P}(-k\boldsymbol{d})$$

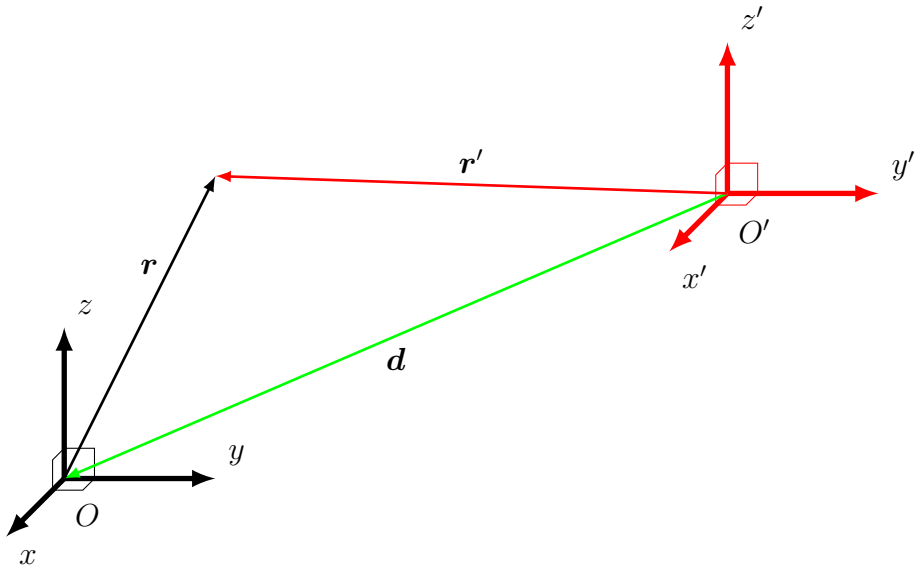

Figure 15: The relation between the translated origins O and O' and the position vectors $\boldsymbol{r}$ and $\boldsymbol{r}'$ at the different origins.

Denote the spherical coordinates of $\boldsymbol{r}$, $\boldsymbol{r}'$, and $\boldsymbol{d}$ by (r,θ,ϕ), (r',θ',ϕ'), and (d,η,ψ), respectively. The translation matrices for a translation $\boldsymbol{d}$ $(d \le 0)$ are [1]

$$\begin{aligned}
\mathcal{P}_{1\sigma ml,1\sigma m'l'}(k\boldsymbol{d}) &= (-1)^{m'} C_{ml,m'l'}(kd,\eta)\cos(m-m')\psi \\
&\quad + (-1)^{\sigma} C_{ml,-m'l'}(kd,\eta)\cos(m+m')\psi \\
\mathcal{P}_{1\sigma ml,1\sigma' m'l'}(k\boldsymbol{d}) &= (-1)^{m'+\sigma'} C_{ml,m'l'}(kd,\eta)\sin(m-m')\psi \\
&\quad + C_{ml,-m'l'}(kd,\eta)\sin(m+m')\psi, \quad \sigma \neq \sigma' \\
\mathcal{P}_{1\sigma ml,2\sigma' m'l'}(k\boldsymbol{d}) &= (-1)^{m'+\sigma} D_{ml,m'l'}(kd,\eta)\cos(m-m')\psi \\
&\quad - D_{ml,-m'l'}(kd,\eta)\cos(m+m')\psi, \quad \sigma \neq \sigma' \\
\mathcal{P}_{1\sigma ml,2\sigma m'l'}(k\boldsymbol{d}) &= (-1)^{m'} D_{ml,m'l'}(kd,\eta)\sin(m-m')\psi \\
&\quad + (-1)^{\sigma} D_{ml,-m'l'}(kd,\eta)\sin(m+m')\psi \\
\mathcal{P}_{2\sigma ml,\tau\sigma' m'l'}(k\boldsymbol{d}) &= \mathcal{P}_{1\sigma ml,\bar{\tau}\sigma' m'l'}(k\boldsymbol{d}), \quad \tau = 1,2
\end{aligned}$$

where

$$\begin{aligned}
C_{ml,m'l'}(kd,\eta) &= \frac{(-1)^{m+m'}}{2}\sqrt{\frac{\varepsilon_m \varepsilon_{m'}}{4}} \\
&\quad \times \sum_{n=|l-l'|}^{l+l'} \mathrm{i}^{l'-l+n}(2n+1)\sqrt{\frac{(2l+1)(2l'+1)(n-(m-m'))!}{l(l+1)l'(l'+1)(n+(m-m'))!}} \\
&\quad \times \begin{pmatrix} l & l' & n \\ 0 & 0 & 0 \end{pmatrix} \begin{pmatrix} l & l' & n \\ m & -m' & m'-m \end{pmatrix} [l(l+1)+l'(l'+1)-n(n+1)] \\
&\quad \times \mathrm{h}_n^{(1)}(kd)\mathrm{P}_n^{m-m'}(\cos\eta)
\end{aligned}$$

$$
\begin{aligned}
D_{ml,m'l'}(kd,\eta) = {} & \frac{(-1)^{m+m'}}{2}\sqrt{\frac{\varepsilon_m\varepsilon_{m'}}{4}} \\
& \times \sum_{n=|l-l'|+1}^{l+l'} \mathrm{i}^{l'-l+n+1}(2n+1)\sqrt{\frac{(2l+1)(2l'+1)(n-(m-m'))!}{l(l+1)l'(l'+1)(n+(m-m'))!}} \\
& \times \begin{pmatrix} l & l' & n-1 \\ 0 & 0 & 0 \end{pmatrix} \begin{pmatrix} l & l' & n \\ m & -m' & m'-m \end{pmatrix} \sqrt{n^2-(l-l')^2} \\
& \times \sqrt{(l+l'+1)^2-n^2}\,\mathrm{h}_n^{(1)}(kd)\mathrm{P}_n^{m-m'}(\cos\eta)
\end{aligned}
$$

where $\varepsilon_m = 2-\delta_{m,0}$ is the Neumann factor, and where $\begin{pmatrix} \cdot & \cdot & \cdot \\ \cdot & \cdot & \cdot \end{pmatrix}$ denotes Wigner's 3j symbol [2], and

$$
(-1)^{\sigma} = \begin{cases} 1, & \sigma = \mathrm{e} \\ -1, & \sigma = \mathrm{o} \end{cases}
$$

Note that the factors $\mathrm{i}^{l'-l+n}$ in $C_{ml,m'l'}(d,\eta)$ and $\mathrm{i}^{l'-l+n+1}$ in $D_{ml,m'l'}(d,\eta)$ are always real numbers, due to the conditions on the Wigner's 3j symbol.

The translation matrix $\mathcal{R}_{nn'}(k\boldsymbol{r})$ is identical to $\mathcal{P}_{nn'}(k\boldsymbol{r})$ but with $\mathrm{h}_n^{(1)}(kd)$ replaced with $\mathrm{j}_n(kd)$.

Appendix C Important integral

In this appendix, we present a recursion algorithm to compute the integral $I_l(z)$. We have

$$
\begin{aligned}
I_l(z) &= \int_0^{\pi} \frac{\mathrm{J}_1(z\sin\theta)}{z\sin\theta}\mathrm{P}_l(\cos\theta)\,\sin\theta\,\mathrm{d}\theta \\
&= \frac{1}{2}\int_0^{\pi} \left(\mathrm{J}_0(z\sin\theta)+\mathrm{J}_2(z\sin\theta)\right)\mathrm{P}_l(\cos\theta)\,\sin\theta\,\mathrm{d}\theta = \frac{1}{2}\left(A_l(z)+B_l(z)\right)
\end{aligned}
$$

The evaluation of the integral $I_l(z)$ is accomplished by computing three integrals, *viz.*,

$$
\begin{cases}
A_l(z) = \displaystyle\int_0^{\pi} \mathrm{J}_0(z\sin\theta)\mathrm{P}_l(\cos\theta)\,\sin\theta\,\mathrm{d}\theta \\
B_l(z) = \displaystyle\int_0^{\pi} \mathrm{J}_2(z\sin\theta)\mathrm{P}_l(\cos\theta)\,\sin\theta\,\mathrm{d}\theta \\
C_l(z) = \displaystyle\int_0^{\pi} \mathrm{J}_2(z\sin\theta)\mathrm{P}_l^2(\cos\theta)\,\sin\theta\,\mathrm{d}\theta
\end{cases}
$$

Only l an even integer gives a non-zero value of these integrals.

The integral representation of the Bessel functions implies

$$
\begin{aligned}
A_l(z) &= \frac{1}{2\pi}\int_0^{2\pi}\int_0^{\pi} \mathrm{e}^{\mathrm{i}z\sin\theta\cos\phi}\mathrm{P}_l(\cos\theta)\,\sin\theta\,\mathrm{d}\theta\,\mathrm{d}\phi \\
&= \frac{1}{2\pi}\iint_{\Omega} \mathrm{e}^{\mathrm{i}z\hat{\boldsymbol{x}}\cdot\hat{\boldsymbol{r}}}\mathrm{P}_l(\hat{\boldsymbol{z}}\cdot\hat{\boldsymbol{r}})\,\mathrm{d}\Omega = 2\mathrm{i}^l\mathrm{j}_l(z)\mathrm{P}_l(0) \quad \text{(C.1)}
\end{aligned}
$$

where we used the integral representation of the spherical Bessel function, see [3, page 638]

$$\mathrm{j}_l(z)\mathrm{Y}_{\sigma ml}(\hat{\boldsymbol{k}}) = \frac{1}{4\pi \mathrm{i}^l} \iint\limits_{\Omega} \mathrm{e}^{\mathrm{i}z\hat{\boldsymbol{k}}\cdot\hat{\boldsymbol{r}}} \mathrm{Y}_{\sigma ml}(\hat{\boldsymbol{r}})\ \mathrm{d}\Omega$$

with $\hat{\boldsymbol{k}} = \hat{\boldsymbol{x}}$, $m = 0$, $\sigma = \mathrm{e}$. Similarly, the integral representation of the Bessel functions implies

$$\begin{aligned} C_l(z) &= -\frac{1}{2\pi} \int_0^{2\pi} \int_0^{\pi} \mathrm{e}^{\mathrm{i}z\sin\theta\cos\phi + 2\mathrm{i}\phi} \mathrm{P}_l^2(\cos\theta)\ \sin\theta\,\mathrm{d}\theta\,\mathrm{d}\phi \\ &= -\frac{1}{2\pi} \int_0^{2\pi} \int_0^{\pi} \mathrm{e}^{\mathrm{i}z\sin\theta\cos\phi} \mathrm{P}_l^2(\cos\theta)\cos 2\phi\ \sin\theta\,\mathrm{d}\theta\,\mathrm{d}\phi = -2\mathrm{i}^l \mathrm{j}_l(z)\mathrm{P}_l^2(0) \end{aligned}$$

with $\hat{\boldsymbol{k}} = \hat{\boldsymbol{x}}$, $m = 2$, $\sigma = \mathrm{e}$.

The integral $C_l(z)$ is now rewritten by the use of the differential equation of the Legendre polynomials. We get

$$\begin{aligned} C_l(z) &= \int_0^{\pi} \mathrm{J}_2(z\sin\theta)(1-\cos^2\theta)\mathrm{P}_l''(\cos\theta)\ \sin\theta\,\mathrm{d}\theta \\ &= \int_0^{\pi} \mathrm{J}_2(z\sin\theta)\left(2\cos\theta\mathrm{P}_l'(\cos\theta) - l(l+1)\mathrm{P}_l(\cos\theta)\right)\ \sin\theta\,\mathrm{d}\theta \\ &= 2\int_0^{\pi} \mathrm{J}_2(z\sin\theta)\cos\theta\,\mathrm{P}_l'(\cos\theta)\ \sin\theta\,\mathrm{d}\theta - l(l+1)B_l(z) \end{aligned} \quad \text{(C.2)}$$

where

$$B_l(z) = \int_0^{\pi} \mathrm{J}_2(z\sin\theta)\mathrm{P}_l(\cos\theta)\ \sin\theta\,\mathrm{d}\theta = \int_{-1}^{1} \mathrm{J}_2(z\sqrt{1-t^2})\mathrm{P}_l(t)\ \mathrm{d}t$$

The first term on the right-hand side in (C.2) is now rewritten as (only $l = 2n$, $n = 1, 2, \ldots$ has a non-zero contribution)

$$\begin{aligned} \int_0^{\pi} \mathrm{J}_2(z\sin\theta)\cos\theta\,\mathrm{P}_{2n}'(\cos\theta)\ \sin\theta\,\mathrm{d}\theta &= \int_{-1}^{1} \mathrm{J}_2(z\sqrt{1-t^2})t\mathrm{P}_{2n}'(t)\ \mathrm{d}t \\ &= \int_{-1}^{1} \mathrm{J}_2(z\sqrt{1-t^2}) \sum_{k=0}^{n} a_k \mathrm{P}_{2k}(t)\ \mathrm{d}t = \sum_{k=0}^{n} a_k B_{2k}(z) \end{aligned}$$

were

$$t\mathrm{P}_{2n}'(t) = \sum_{k=0}^{n} a_k \mathrm{P}_{2k}(t) \quad \text{(C.3)}$$

The coefficients a_k are determined by ($n = 1, 2, \ldots$)

$$a_k = \frac{4k+1}{2} \int_{-1}^{1} t\mathrm{P}_{2n}'(t)\mathrm{P}_{2k}(t)\ \mathrm{d}t, \quad k = 0, 1, 2, \ldots, n$$

The special value at $k = 0$ is first addressed.

$$a_0 = \frac{1}{2}\int_{-1}^{1} \mathrm{P}_1(t)\mathrm{P}'_{2n}(t)\ \mathrm{d}t = 1, \quad n = 1, 2, \ldots$$

since, see [3, (C.1) on page 623]

$$\int_{-1}^{1} \mathrm{P}'_{2n}(t)\mathrm{P}_{2m+1}(t)\ \mathrm{d}t = 2(1 - \delta_{mn}), \quad m = 0, 1, 2, \ldots, n \tag{C.4}$$

All other coefficients a_k are computed by employing the recursion relations of the Legendre polynomials. We get

$$a_k = \frac{1}{2}\int_{-1}^{1} \mathrm{P}'_{2n}(t)\left((2k+1)\mathrm{P}_{2k+1}(t) + 2k\mathrm{P}_{2k-1}(t)\right)\ \mathrm{d}t, \quad k = 1, 2, \ldots, n$$

since [3, page 622]

$$(4k+1)t\mathrm{P}_{2k}(t) = (2k+1)\mathrm{P}_{2k+1}(t) + 2k\mathrm{P}_{2k-1}(t)$$

and we obtain by (C.4)

$$a_k = (2k+1)(1 - \delta_{nk}) + 2k = 4k + 1 - (2n+1)\delta_{nk}$$

In particular, we get

$$a_k = 4k + 1, \quad k = 0, 1, 2, \ldots, n-1, \qquad a_n = 2n$$

and the sum in (C.3) becomes

$$t\mathrm{P}'_{2n}(t) = \sum_{k=0}^{n-1}(4k+1)\mathrm{P}_{2k}(t) + 2n\mathrm{P}_{2n}(t), \quad n = 1, 2, \ldots$$

Consequently, from (C.2), the integrals $B_l(z)$ are related by

$$2\sum_{k=1}^{n} a_k B_{2k}(z) - 2n(2n+1)B_{2n}(z) = 2b_n(z), \quad n = 1, 2, \ldots$$

where

$$\begin{aligned} b_n(z) = -(-1)^n \mathrm{j}_{2n}(z)\mathrm{P}^2_{2n}(0) &= \frac{\mathrm{j}_{2n}(z)(2n+2)!}{2^{2n}(n+1)!(n-1)!} \\ &= \frac{\mathrm{j}_{2n}(z)(2n+2)!}{(2n+2)!!(2n-2)!!} = \frac{\mathrm{j}_{2n}(z)(2n+1)!!}{(2n-2)!!}, \quad n = 1, 2, \ldots \end{aligned}$$

The first terms are

$$b_0(z) = 0, \quad b_1(z) = 3\mathrm{j}_2(z)$$

Rewrite the iteration scheme above as

$$B_{2n}(z) = \frac{1}{n(2n-1)} \sum_{k=0}^{n-1} (4k+1) B_{2k}(z) - \frac{b_n(z)}{n(2n-1)}, \quad n = 1, 2, \ldots$$

The relation between two iterations is

$$B_{2n+2}(z) = \frac{1}{(n+1)(2n+1)} \sum_{k=0}^{n} (4k+1) B_{2k}(z) - \frac{b_{n+1}(z)}{(n+1)(2n+1)}$$

or

$$\begin{aligned} B_{2n+2}(z) &= \frac{4n+1}{(n+1)(2n+1)} B_{2n}(z) \\ &\quad + \frac{1}{(n+1)(2n+1)} \sum_{k=0}^{n-1} (4k+1) B_{2k}(z) - \frac{b_{n+1}(z)}{(n+1)(2n+1)} \\ &= \frac{4n+1}{(n+1)(2n+1)} B_{2n}(z) + \frac{n(2n-1)}{(n+1)(2n+1)} \left(B_{2n}(z) + \frac{b_n(z)}{n(2n-1)} \right) \\ &\quad - \frac{b_{n+1}(z)}{(n+1)(2n+1)} \end{aligned}$$

The final iteration scheme is

$$B_{2n+2}(z) = B_{2n}(z) + \frac{b_n(z) - b_{n+1}(z)}{(n+1)(2n+1)} = B_{2n}(z) + \beta_n(z), \quad n = 0, 1, 2, \ldots$$

where

$$\beta_n(z) = \frac{b_n(z) - b_{n+1}(z)}{(n+1)(2n+1)}, \quad n = 0, 1, 2, \ldots$$

The solution of the iteration scheme is

$$B_{2n}(z) = B_0(z) + \sum_{k=0}^{n-1} \beta_n(z), \quad n = 1, 2, \ldots \tag{C.5}$$

The start value of the iteration is (not generated by the iterations scheme)

$$B_0(z) = 2 \int_0^1 \mathrm{J}_2(z\sqrt{1-t^2})\, \mathrm{d}t = 2 \int_0^1 \frac{u \mathrm{J}_2(zu)}{\sqrt{1-u^2}}\, \mathrm{d}u = \frac{4 - 4\cos z - 2z \sin z}{z^2}$$

and for $n = 1$ in (C.5)

$$B_2(z) = B_0(z) + \beta_0(z) = B_0(z) - 3\mathrm{j}_2(z)$$

As a check, the explicit integral can also be computed.

$$B_2(z) = \int_0^1 \mathrm{J}_2(z\sqrt{1-t^2})(3t^2 - 1)\, \mathrm{d}t = \frac{4z + 5z\cos z - 9\sin z}{z^3} + \frac{\sin z}{z}$$

The final integral $I_l(z)$ is now solved. We have

$$I_{2n}(z) = \int_0^\pi \frac{\mathrm{J}_1(z\sin\theta)}{z\sin\theta}\mathrm{P}_{2n}(\cos\theta)\,\sin\theta\,\mathrm{d}\theta$$
$$= \frac{1}{2}\int_0^\pi \left(\mathrm{J}_0(z\sin\theta) + \mathrm{J}_2(z\sin\theta)\right)\mathrm{P}_{2n}(\cos\theta)\,\sin\theta\,\mathrm{d}\theta = \frac{1}{2}\left(A_{2n}(z) + B_{2n}(z)\right)$$

The first value is

$$I_2(z) = \frac{1}{2}\left(A_2(z) + B_2(z)\right) = \frac{z(2+\cos z) - 3\sin z}{z^3}$$

In summary, the integral $I_l(z) = (A_l(z) + B_l(z)/2$ is computed by (C.1) and (C.5) and the value of $B_0(z)$.

References

[1] A. Boström, G. Kristensson, and S. Ström. Transformation properties of plane, spherical and cylindrical scalar and vector wave functions. In V. V. Varadan, A. Lakhtakia, and V. K. Varadan, editors, *Field Representations and Introduction to Scattering*, Acoustic, Electromagnetic and Elastic Wave Scattering, chapter 4, pages 165–210. Elsevier Science Publishers, Amsterdam, 1991.

[2] A. R. Edmonds. *Angular Momentum in Quantum Mechanics.* Princeton University Press, Princeton, NJ, 3 edition, 1974.

[3] G. Kristensson. *Scattering of Electromagnetic Waves by Obstacles.* Mario Boella Series on Electromagnetism in Information and Communication. SciTech Publishing, Edison, NJ, USA, 2016.

[4] F. W. J. Olver, D. W. Lozier, R. F. Boisvert, and C. W. Clark. *NIST Handbook of mathematical functions.* Cambridge University Press, New York, 2010.